ORGANOMETALLICS
Article

Organometallics **2010,** *29,* 1629–1641 1629
DOI: 10.1021/om901023n

Carbonyl Complexes of Rhodium with N-Donor Ligands: Factors Determining the Formation of Terminal versus Bridging Carbonyls

Wojciech I. Dzik,[†] Charlotte Creusen,[‡] René de Gelder,[‡] Theo P. J. Peters,[‡] Jan M. M. Smits,[‡] and Bas de Bruin*,[†]

[†]*Department of Homogeneous and Supramolecular Catalysis, Van't Hoff Institute for Molecular Sciences (HIMS), University of Amsterdam, Nieuwe Achtergracht 166, 1018 WV Amsterdam, The Netherlands, and* [‡]*Institute for Molecules and Materials, Radboud Universiteit Nijmegen, Heyendaalseweg 135, 6525 AJ Nijmegen, The Netherlands*

Received November 25, 2009

Cationic rhodium carbonyl complexes supported by a series of different N_3- and N_4-donor ligands were prepared, and their ability to form carbonyl-bridged species was evaluated. Complex [Rh(κ^3-bpa)(cod)]$^+$ (**1**$^+$) (bpa = bis(2-picolyl)amine, cod = *cis*,*cis*-1,5-cyclooctadiene) reacts with 1 bar of CO to form a tris-carbonyl-bridged species [Rh_2(κ^3-bpa)$_2$(μ-CO)$_3$]$^{2+}$ (**2**$^{2+}$), which in solution slowly decomposes to the terminal monocarbonyl complex [Rh(κ^3-bpa)(CO)]$^+$ (**3**$^+$). Similar conditions lead to direct formation of a terminal monocarbonyl species, [Rh(κ^3-Bu-bpa)(CO)]$^+$ (**5**$^+$), from [Rh(κ^3-Bu-bpa)(cod)]$^+$ (**4**$^+$) (Bu-bpa = *N*-butylbis(2-picolyl)amine). Treatment of **4**$^+$ with 50 bar of CO leads to only partial conversion (~15%) to the tris-carbonyl-bridged species [Rh_2(κ^3-Bu-bpa)$_2$(μ-CO)$_3$]$^{2+}$ (**6**$^{2+}$). Stabilization of tris-carbonyl bridges can be achieved by cooperative binding. Tethering two bpa moieties with a propylene linker allows cooperative CO binding to [(CO)Rh(μ-(bis-κ^3)tppn)Rh(CO)]$^{2+}$, producing the tetranuclear complex [Rh_4(μ-(bis-κ^3)tppn)$_2$((μ-CO)$_3$)$_2$]$^{4+}$ (**13**)$^{4+}$ at 50 bar of CO (tppn = tppn = N^1,N^1,N^2,N^2-tetrakis(pyridin-2-ylmethyl)propane-1,2-diamine). Tetranuclear complex **13**$^{4+}$ is stable at room temperature in the absence of CO (in contrast to binuclear Rh(μ_2-CO)$_3$Rh-bridged complex **6**$^{2+}$). In solution, the cationic rhodium carbonyl complex [Rh(κ^3-tpa)(CO)]$^+$ (**14**$^+$) (containing the N_4-donor ligand tpa = tris(2-picolyl)amine)) exists in dynamic equilibrium with the dinuclear bis-carbonyl-bridged species [Rh(κ^4-tpa)(μ-CO)]$_2^{2+}$ (**15**$^{2+}$). Remarkably, the bis-carbonyl-bridged Rh(μ_2-CO)$_2$Rh motive in **15**$^{2+}$ is not supported by a Rh−Rh bond or other bridging ligands. The thermodynamic parameters for dimerization of **14**$^+$ to **15**$^{2+}$ in acetone were measured ($\Delta H° = -28.4 \pm 1.7$ kJ·mol^{-1} and $\Delta S° = -134 \pm 7$ J·mol·K^{-1}). Formation of bis-carbonyl-bridged species was not observed with the weaker Me_3tpa ligand. The stability of the bis- and tris-carbonyl-bridged structures clearly depends on a delicate balance between the favorable enthalpy (enhanced with stronger σ-donor ligands) and unfavorable entropy (that can be reduced by multivalent binding) associated with their formation. In the solid state complex **14**$^+$ reacts selectively with dioxygen to form a carbonato complex, [Rh(κ^4-tpa)(CO_3)]$^+$ (**16**$^+$).

Introduction

Carbonyl complexes of rhodium with the tridentate nitrogen-donor "scorpionato" trispyrazolyl (Tp) type of ligands have received much attention over the past two decades.[1] It was shown that complexes of the type Rh(Tp*)(CO)$_2$ (Tp* = tris(3,5-dimethylpyrazolyl)borate) photochemically activate C−H bonds of alkanes,[2] show a high degree of fluxionality in solution,[3] and reveal interesting one-electron redox properties in the presence of a supporting phosphorus ligand.[4]

The arrangement of the pyrazolyl moieties of the Tp-type ligands imposes a *fac*-coordination mode.[1] Furthermore, Rh^I complexes with Tp-type ligands reveal a hemilabile coordination mode with the κ^2−κ^3 equilibrium producing diverse structures spanning from mononuclear square-planar and trigonal-bypiramidal or square-pyramidal bis-carbonyls,[5] to octahedral dinuclear

*Corresponding author. E-mail: b.debruin@uva.nl.

(1) For a review on trispyrazolyl borate rhodium complexes see: Slugovc, C.; Padilla-Martínez, I.; Sirol, S.; Carmona, E. *Coord. Chem. Rev.* **2001**, *213*, 129–157.

(2) (a) Ghosh, C. K.; Graham, W. A. G. *J. Am. Chem. Soc.* **1987**, *109*, 4726–4727. (b) Bromberg, S. E.; Yang, H.; Asplund, M. C.; Lian, T.; McNamara, B. K.; Kotz, K. T.; Yeston, J. S.; Wilkens, M.; Frei, H.; Bergman, R. G.; Harris, C. B. *Science* **1997**, *278*, 260–263.

(3) Webster, C. E.; Hall, M. B. *Inorg. Chim. Acta*, **2002**, *330*, 268−282, and references therein.

(4) For examples see: (a) Connelly, N. G.; Emslie, D. J. H.; Geiger, W. E.; Hayward, O. D.; Linehan, E. B.; Orpen, A. G.; Quayle, M. J.; Rieger, P. H. *J. Chem. Soc., Dalton Trans.* **2001**, 670–683. (b) Geiger, W. E.; Camire Ohrenberg, N.; Yeomans, B.; Connelly, N. G.; Emslie, D. J. H. *J. Am. Chem. Soc.* **2003**, *125*, 8680–8688.

(5) Compounds characterized by X-ray diffraction: (a) Rheingold, A. L.; Liable-Sands, L. M.; Incarvito, C. L.; Trofimenko, S. *J. Chem. Soc., Dalton. Trans.* **2002**, 2297–2301. (b) Adams, C. J.; Connelly, N. G.; Emslie, D. J.; Hayward, O. D.; Manson, T.; Orpen, A. G.; Rieger, P. H. *Dalton. Trans.* **2003**, 2835–2845. (c) Rheingold, A. L.; Liable-Sands, L. M.; Golan, J. A..; Trofimenko, S. *Eur. J. Inorg. Chem.* **2003**, 2767–2773. (d) Blake, A. J.; George, M. W.; Hall, M. B.; McMaster, J.; Portius, P.; Sun, X. Z.; Towrie, M.; Webster, C. E.; Wilson, C.; Zarić, S. D. *Organometallics* **2008**, *27*, 189–201.

Published on Web 03/10/2010

Scheme 1. Different Coordination Behavior of Trispyrazolyl Ligands X = BH, CH, GaMe

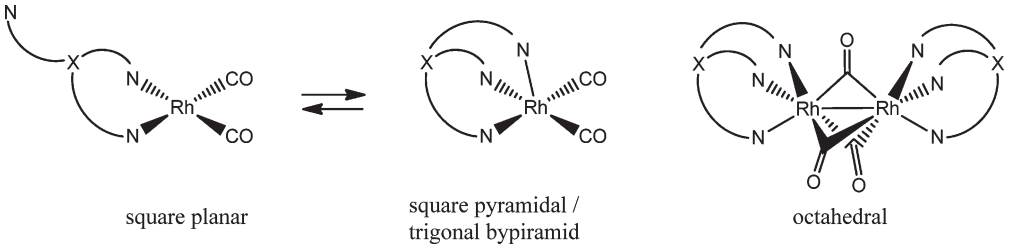

triscarbonyl-bridged[6] species (Scheme 1). Similar structures (although $\kappa^2-\kappa^3$ isomerism was not reported) were found for cyclic *fac*-coordinating tri-[7] and hexa-amines,[8] with the latter ones forming supramolecular, tris-carbonyl-bridged tetranuclear assemblies.

While these strictly *fac*-coordinating N-donor ligands have been thoroughly studied, surprisingly little attention has been given to rhodium carbonyl complexes with more flexible podal N-donor ligands that can adopt both *fac*- and *mer*-coordination modes.

Mathieu and Ros reported that bis[(3,5-dimethyl-1-pyrazolyl)methyl]ethylamine can bind in both fashions to a cationic rhodium carbonyl center, resulting in formation of either monocarbonyl square-planar or bis-carbonyl square-pyramidal complexes (Scheme 2).[9] The factors that determine the coordination mode of the N-donor ligand and as a result the number of carbonyl ligands per metal atom were not investigated.

The above structural diversity of N-donor ligand Rh-carbonyl complexes is intriguing and could well result in different reactivities. For this reason we became interested in the factors that determine the coordination mode of both the carbonyl ligands and the N-donor ligands in cationic $[\{Rh(CO)_x(\text{N-donor ligand})\}_y]^{y+}$ complexes with flexible podal N-donor ligands.

Scheme 2. *mer*- and *fac*-Coordination of a N_3 Ligand toward Rhodium Carbonyl

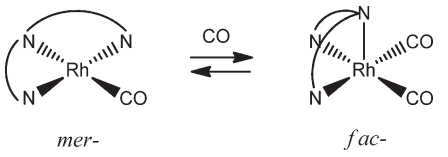

Scheme 3. Ligands Used in This Study

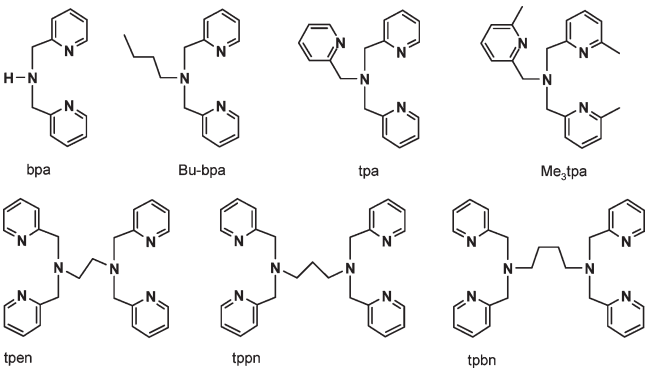

Given the rich chemistry of rhodium olefin complexes with bispicolylamine (bpa)-type ligands[10,11] and dual *fac*- and *mer*-coordination behavior of bpa, we were especially interested in the coordination modes of the flexible ligands shown in Scheme 3 and understanding the factors that drive the formation of mononuclear complexes with terminal carbonyl ligands versus binuclear carbonyl-bridged complexes.

Bridging carbonyl complexes are frequently "resting state" or "dead end" species in several catalytic carbonylation reactions (e.g., hydroformylation),[12,13] and therefore a better understanding of the factors that determine their formation might well be of synthetic relevance.

Results and Discussion

For the tridentate bpa type of ligands we compared the Bu-bpa ligand having a butyl substituent on the central amine donor with the nonfunctionalized bpa ligand to investigate

(6) Compound characterized by X-ray diffraction: (a) Methyl-(trispyrazol-1-yl)gallate: Louie, B. M.; Rettig, S. J.; Storr, A.; Trotter, J. *Can. J. Chem.* **1984**, *62*, 633–637. Other examples: (b) Tris-(2-pyridy1)phosphineoxide ligand: Cesares, J. A.; Espinet, P.; Martín-Alvarez, J. M.; Espino, G.; Pérez-Manrique, M.; Vattier, F. *Eur. J. Inorg. Chem.* **2001**, 289–296. (c) Tris(pyrazol-1-yl)methane: Estruelas, M. A.; Oro, L. A.; Claramunt, R. M.; López, C.; Lavandera, J. L.; Elguero, J. *J. Organomet. Chem.* **1989**, *366*, 245–255. (d) Tris(pyrazol-1-yl)borate: O'Sullivan, D. J.; Lalor, F. J. *J. Organomet. Chem.* **1974**, *65*, C47–49. (e) Cocivera, M.; Desmond, T. J.; Ferguson, G.; Kaitner, B.; Lalor, F. J.; O'Sullivan, D. J. *Organometallics* **1982**, *1*, 1125. (f) Tris(pyrazol-1-yl)methanesulfonate: Kläui, W.; Schramm, D.; Peters, W.; Rheinwald, G.; Lang, H. *Eur. J. Inorg. Chem.* **2001**, 1415–1424.

(7) Compound characterized by X-ray diffraction: de Bruin, B.; Donners, J. J. J. M.; de Gelder, R.; Smits, J. M. M.; Gal, A. W. *Eur. J. Inorg. Chem.* **1998**, 401–406.

(8) Compounds characterized by X-ray diffraction: (a) Macrocyclic hexamines: Lecomte, J.-P.; Lehn, J.-M.; Parker, D.; Guilheim, J.; Pascard, C. *J. Chem. Soc., Chem. Commun.* **1983**, 296–298. (b) Johnson, J. M.; Bulkowski, J. E.; Rheingold, A. L.; Gates, B. C. *Inorg. Chem.* **1987**, *26*, 2644–2646. Other representative example: (c) Parker, D. *J. Chem. Soc., Chem. Commun.* **1985**, 1129–1131.

(9) Mathieu, R.; Esquius, G.; Lugan, N.; Pons, J.; Ros, J. *Eur. J. Inorg. Chem.* **2001**, 2683–2688.

(10) (a) Tejel, C.; Ciriano, M. A.; del Río, M. P.; van den Bruele, F. J.; Hetterscheid, D. G. H.; Tsichlis i Spithas, N.; de Bruin, B. *J. Am. Chem. Soc.* **2008**, *130*, 5844–5845. (b) Hetterscheid, D. G. H.; Klop, M.; Kicken, R. J. N. A. M.; Smits, J. M. M.; Reijerse, E. J.; de Bruin, B. *Chem.—Eur. J.* **2007**, *13*, 3386–3405. (c) de Bruin, B.; Verhagen, J. A. W.; Schouten, C. H. J.; Gal, A. W.; Feichtinger, D.; Plattner, D. A. *Chem.—Eur. J.* **2001**, *7*, 416–422.

(11) de Bruin, B.; Brands, J. A.; Donners, J. J. J. M.; Donners, M. P. J.; de Gelder, R.; Smits, J. M. M.; Gal, A. W.; Spek, A. L. *Chem.—Eur. J.* **1999**, *5*, 2921–2936.

(12) van Leeuwen, P. W. N. M., Claver C., Eds. *Rhodium Catalyzed Hydroformylation*; Kluwer Acedemic Publishers: Dordrecht, 2000.

(13) Formation of μ^2-carbonyl-bridged rhodium dimers with terminal carbonyls was reported for some hydroformylation catalysts: (a) Wilkinson's catalyst: Evans, D.; Yagupsky, G.; Wilkinson, G. *J. Chem. Soc. A* **1968**, 2660–2665. (b) Chan, A. S. C.; Shieh, H. S.; Hill, J. R. *J. Chem. Soc., Chem. Commun.* **1983**, 688–689. (c) Diphosphines: James, B. R.; Mahajan, S. J.; Rettig, G. M. Williams *Organometallics* **1983**, *2*, 1452–1458. (d) Castellanos-Páez, A.; Castillón, S.; Claver, C.; van Leeuwen, P. W. N. M.; de Lange, W. G. J. *Organometallics* **1998**, *17*, 2543–2552. (e) Diphosphites: Buisman, G. J. H.; van der Veen, L. A.; Kamer, P. C. J.; van Leeuwen, P. W. N. M. *Organometallics* **1997**, *16*, 5681–5687.

Scheme 4. Synthesis of $[Rh_2(\kappa^3\text{-bpa})_2(\mu\text{-CO})_3]^{2+}$ ($\mathbf{2}^{2+}$) and $[Rh(\kappa^3\text{-bpa})(CO)]^{+}$ ($\mathbf{3}^{+}$)

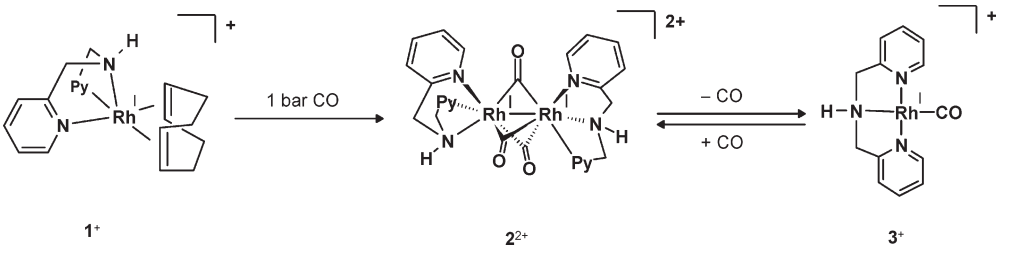

the influence of the electronic effects (stronger bpa donor vs weaker Bu-bpa)[14] on the formation of mononuclear terminal versus bridging carbonyl complexes (Scheme 3). We also prepared ditopic alkyl-bpa-bridged complexes with an alkyl tether between two bpa units in an attempt to lower the unfavorable entropic factors associated with the formation of bridged carbonyl complexes. For the tetradentate tpa-type ligands we compared the stronger nonfunctionalized tpa donor with the Me_3tpa donor bearing methyl substituents on the pyridine-6 positions (Scheme 3). These substituents have some steric influence on the metal coordination, which results in the pyridine units being weaker donors to the metal compared with nonsubstituted pyridines.[11]

Rhodium Carbonyl Complexes with Bis(picolyl)amine and *N*-Butyl(bis(picolyl)amine). Reaction of $[Rh(\kappa^3\text{-bpa})(\eta^4\text{-cod})]PF_6$ ([**1**]PF_6) (cod = *cis*,*cis*-1,5-cyclooctadiene) with CO at a pressure of 1 bar in dichloromethane results in formation of the tris-carbonyl-bridged binuclear complex $[Rh_2(\kappa^3\text{-bpa})_2(\mu\text{-CO})_3](PF_6)_2$ ([**2**]$(PF_6)_2$) (Scheme 4). The complex has C_2 symmetry and is not fluxional in solution on the NMR time scale, which results in separate NMR signals of the inequivalent pyridine and methylene groups of the bpa ligand. The inequivalence is a result of the coordination mode in which two CO ligands are *trans* to picolyl and amine moieties, whereas the third CO is *trans* to the two picolyl groups of the different bpa ligands. This coordination mode is similar to that previously reported for $[Rh_2(\mu\text{-CO})_3Cl_2(Py)_2]$[15] and was confirmed by single-crystal X-ray diffraction. The crystal was grown by top layering an acetone solution of [**2**]$(PF_6)_2$ with hexanes at −20 °C. Although the quality of the crystal data is hampered by severe PF_6 disorder, the molecular structure of the dication $\mathbf{2}^{2+}$ is unambiguously revealed by the X-ray data. See Figure 1.

The IR spectrum of the carbonyl region reveals two overlapping bands at 1835 and 1828 cm^{-1}, and ^{13}C NMR reveals two triplets of intensity 2:1 at 215.8 and 210.4 ppm, with Rh−C coupling constants of 28.4 and 27.9 Hz, respectively. This complex is stable in the solid state for at least 2 months. In solution it slowly converts to the monocarbonyl complex $[Rh(\kappa^3\text{-bpa})(\eta^1\text{-CO})]PF_6$ ([**3**]PF_6) (approximately 30% conversion in acetone after 10 days, heating under reflux in acetone for 2 h leads to quantitative conversion) (Scheme 4). Complex $\mathbf{3}^{+}$ reveals a single CO stretching band at 1989 cm^{-1} and ^{13}C NMR resonance at 190.3 ppm with a Rh−C coupling constant of 77.5 Hz in MeCN.

In marked contrast to its bpa analogue, reaction of the $[(\kappa^3\text{-Bu-bpa})Rh^{I}(\eta^4\text{-cod})]PF_6$ complex ([**4**]PF_6) with 1 bar of CO does not lead to a binuclear, tris-carbonyl-bridged species analogous to $\mathbf{2}^{2+}$. Instead, treatment of [**4**]PF_6 with 1 bar of CO in CH_3CN or CH_2Cl_2 results directly in a clean and facile substitution of cod by CO with formation of only the square-planar carbonyl complex $[(\kappa^3\text{-Bu-bpa})Rh(CO)]PF_6$ ([**5**]PF_6) (Scheme 5). In the conversion of the η^4-cod to the monocarbonyl complexes the coordination mode of the Bu-bpa ligand changes from *fac* to *mer*, as evidenced

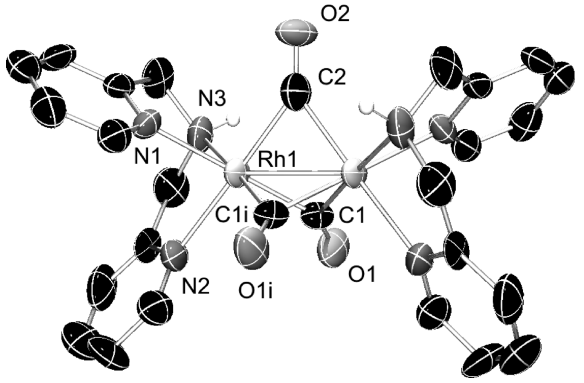

Figure 1. X-ray structure of $[Rh_2(\kappa^3\text{-bpa})_2(\mu\text{-CO})_3]^{2+}$ ($\mathbf{2}^{2+}$). Thermal ellipsoids are drawn with 50% probability. Hydrogen atoms bound to the carbon atoms, the PF_6^- counterions, and acetone molecules are omitted for clarity. Selected bond lengths [Å] and angles [deg]: Rh(1)−C(1) 2.004(14); Rh(1)−C(1i) 2.019(12); Rh(1)−C(2) 2.019(18); Rh(1)−N(1) 2.165(11); Rh(1)−N(2) 2.176(12); Rh(1)−N(3) 2.184(12); Rh(1)−Rh(1i) 2.5710(18); C(1)−O(1) 1.140(16); C(2)−O(2) 1.14(2); C(1)−Rh(1)−C(1i) 82.1(6); C(1)−Rh(1)−C(2) 84.6(5); C(1i)−Rh(1)−C(2) 84.2(5); C(1)−Rh(1)−N(1) 177.4(5); C(1i)−Rh(1)−N(1) 100.5(5); C(2)−Rh(1)−N(1) 96.0(4); C(1)−Rh(1)−N(2) 95.2(5); C(1i)−Rh(1)−N(2) 99.3(5); C(2)−Rh(1)−N(2) 176.5(5); N(1)−Rh(1)−N(2) 84.1(4); C(1)−Rh(1)−N(3) 98.6(5); C(1i)−Rh(1)−N(3) 177.5(5); C(2)−Rh(1)−N(3) 98.3(5); N(1)−Rh(1)−N(3) 78.9(4); N(2)−Rh(1)−N(3) 78.2(5); Rh(1)−C(1)−Rh(1i) 79.5(4); Rh(1i)−C(2)−Rh(1) 79.1(8).

Scheme 5. Synthesis of $[Rh(\kappa^3\text{-Bu-bpa})(CO)]^{+}$ ([5**]$^{+}$)**

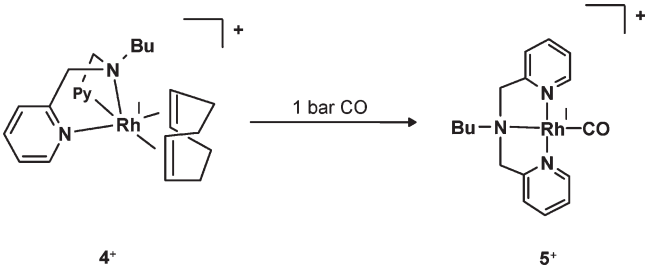

(14) The weaker donor strength of alkyl-bpa derivatives is caused by steric effects. See ref 11.

(15) Heaton, B. T.; Jacob, C.; Sampanthar, J. T. *J. Chem. Soc., Dalton Trans.* **1998**, 1403–1410.

Scheme 6. Reaction of [Rh(κ^3-Bu-bpa)(CO)]$^+$ ($\mathbf{5}^+$) with 50 bar of CO to Form [Rh$_2$(κ^3-Bu-bpa)$_2$(μ-CO)$_3$]$^{2+}$ ($\mathbf{6}^{2+}$) and [Rh(κ^3-Bu-bpa)(CO)$_2$]$^+$ ($\mathbf{7}^+$)

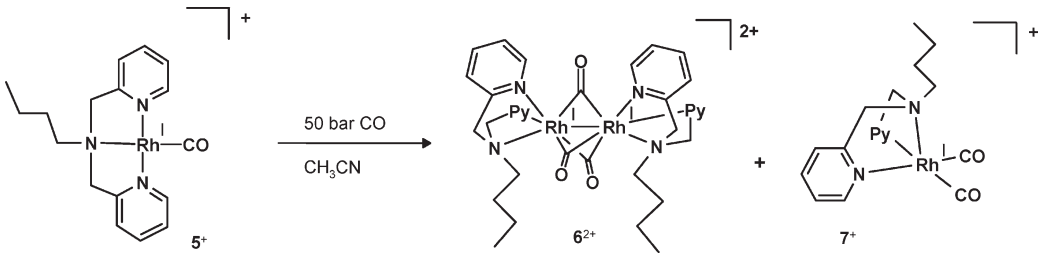

by NOESY measurements.[16] Cation $\mathbf{5}^+$ is also obtained by reaction of Bu-bpa and [{(CO)$_2$Rh(μ-Cl)}$_2$] in a 2:1 molar ratio in MeOH followed by addition of NH_4PF_6, which produces [**5**]PF_6 as a yellow precipitate.

The substantially different stabilities of the Rh(μ-CO)$_3$Rh-bridged complexes with bpa versus Bu-bpa are remarkable, considering the structural resemblance of these ligands. We thus wondered if we could enforce the formation of Rh(μ-CO)$_3$Rh with the Bu-bpa ligand at higher CO pressures.

Treatment of [**5**]PF_6 with 50 bar of CO for approximately 7 days results in partial conversion (approximately 15%) to a mixture of the dinuclear, dicationic complex [Rh$_2$(κ^3-Bu-bpa)$_2$(μ-CO)$_3$](PF_6)$_2$ ([**6**](PF_6)$_2$) and mononuclear, monocationic complex Rh[(κ^3-Bu-bpa)(CO)$_2$]PF_6 ([**7**](PF_6)), containing two terminal CO ligands, as was observed by mass spectrometry and IR spectroscopy (Scheme 6).[17]

FAB-MS (m/z = 945, 917) and FT-IR spectra ($\nu_{(CO)}$ = 1832 cm^{-1} (KBr)) of $\mathbf{6}^{2+}$ are in accordance with the tris-μ-carbonyl-bridged structure, while m/z 772 and $\nu_{(CO)}$ = 1992 and 2042 cm^{-1} confirm the presence of the bis-carbonyl complex $\mathbf{7}^+$. Attempts to prepare [**6**](PF_6)$_2$ in high yield were unsuccessful, which might indicate an equilibrium between $\mathbf{6}^{2+}$ and $\mathbf{5}^+$ in the presence of CO. In accordance with this, [**6**](PF_6)$_2$ is not stable in the solid state at room temperature in the absence of CO and converts to [**5**]PF_6 within days. Heating of the isolated mixture of [**5**]PF_6 and [**6**](PF_6)$_2$ in acetonitrile to 50 °C for 2 h results in full conversion of the contained [**6**](PF_6)$_2$ to [**5**]PF_6.

It is difficult to imagine that substitution of a proton for a butyl group will have any significant steric influence on the formation of the Rh(μ-CO)$_3$Rh bridge (tethered alkyl-substituted bpa complexes do form carbonyl-bridged species, *vide infra*). Therefore, the markedly different stability of the dirhodium tris-carbonyl species $\mathbf{2}^{2+}$ and $\mathbf{6}^{2+}$ is most likely caused by the decrease in donor capacity of the ligand on going from bpa to Bu-bpa. The more electron-rich rhodium atom of bpa complex $\mathbf{2}^{2+}$ is expected to bind CO more strongly than the Bu-bpa-ligated metal in the complex $\mathbf{6}^{2+}$, which should result in relative stabilization of the (μ-CO)$_3$ bridge in $\mathbf{2}^{2+}$ compared to $\mathbf{6}^{2+}$.

Table 1. IR and ^{13}C NMR Spectroscopy Data of the Carbonyl Ligands

complex	$\nu_{(C\equiv O)}$ solution [cm^{-1}]	$\nu_{(C\equiv O)}$ solid state [cm^{-1}]	^1J(Rh,C) [Hz]
[Rh$_2$(bpa)$_2$(μ-CO)$_3$]$^{2+}$ ($\mathbf{2}^{2+}$)	1835 (shoulder at 1828)	1836, 1815	28.4, 27.9
[Rh(bpa)(CO)]$^+$ ($\mathbf{3}^+$)	1989		77.5
[Rh(Bu-bpa)(CO)]$^+$ ($\mathbf{5}^+$)	1994		79.1
[Rh$_2$(Bu-bpa)$_2$(μ-CO)$_3$]$^{2+}$ ($\mathbf{6}^{2+}$)		1832	
[Rh(Bu-bpa)(CO)$_2$]$^+$ ($\mathbf{7}^+$)		1992, 2042	
[Rh$_2$(tpen)(CO)$_2$]$^{2+}$ ($\mathbf{11}^{2+}$)	1999		67.5
[Rh$_2$(tppn)(CO)$_2$]$^{2+}$ ($\mathbf{12}^{2+}$)	1994		79.0
[Rh$_2$(tppn)(μ-CO)$_3$]$_2^{4+}$ ($\mathbf{13}^{4+}$)	1838 (shoulder at 1828)		29.1, 29.1
[Rh$_2$(tpbn)(CO)$_2$]$^{2+}$		1992	
[Rh$_2$(tpbn)(CO)$_2$]$_n^{2+}$		1843	
[Rh(tpa)(CO)]$^+$ ($\mathbf{14}^+$)	1991	1985	79.5
[Rh(tpa)(μ-CO)]$_2^{2+}$ ($\mathbf{15}^{2+}$)	1749	1740	19.6

The CO stretch frequencies of the square-planar complexes $\mathbf{3}^+$ and $\mathbf{5}^+$ (1989 vs 1994 cm^{-1} for bpa and Bu-bpa, respectively) confirm that Bu-bpa is indeed a weaker donor than bpa (Table 1). Although the difference in stretch frequencies (5 cm^{-1}) does not seem to be large, it is significant and might explain the different relative stability of the bridged carbonyl complexes $\mathbf{2}^{2+}$ and $\mathbf{6}^{2+}$.

Synthesis and Structure of Cyclooctadiene and Carbonyl Rhodium Complexes with Tethered bpa Ligands. Concluding that the Bu-bpa complex $\mathbf{6}^{2+}$ is thermodynamically unstable, we decided to investigate if the tris-carbonyl-bridged species could be stabilized by cooperative binding of binuclear rhodium bpa species tethered with an alkyl chain. We expected that the reduction of the entropy of binding by tethering of the rhodium carbonyl complexes could lead to structures similar to the reported hexamine macrocylic tris-carbonyl-bridged rhodium complexes.[8] For that reason we synthesized corresponding cod and carbonyl complexes with ligands that have bpa moieties tethered by a chain of two, three, and four carbon atoms and investigated their reactivity with CO.

[Rh$_2$((μ-(bis-κ^3)tpen)$_2$(η^4-cod)$_2$](PF_6)$_2$ ([**8**](PF_6)$_2$), [Rh$_2$((μ-(bis-κ^3)tppn)(η^4-cod)$_2$](PF_6)$_2$ ([**9**](PF_6)$_2$), and the previously reported [Rh$_2$((μ-(bis-κ^3)tpbn)(η^4-cod)$_2$](PF_6)$_2$[11] ([**10**](PF_6)$_2$) (tpen = N^1,N^1,N^2,N^2-tetrakis(pyridin-2-ylmethyl)ethane-1,2-diamine, tppn = N^1,N^1,N^2,N^2-tetrakis(pyridin-2-ylmethyl)-propane-1,2-diamine, tpbn = N^1,N^1,N^2,N^2-tetrakis(pyridin-2-ylmethyl)butane-1,2-diamine) were synthesized by reacting [Rh(μ-Cl)(η^4-cod)]$_2$ with the corresponding N_3-donor ligands

(16) In the ^{1}H-NOESY spectrum of [(Bu-bpa)Rh$^{\mathrm{I}}$(CO)]$^+$ ([**2**]$^+$), clear NOE contacts are observed between the α-CH_2-group of the butylamine fragment (N-CH_2-Pr) and the equatorial N-CH_2-Py protons (one of the two AB-type doublets). The latter also show NOE contacts with Py-H3. The axial N-CH_2-Py protons (other AB-type doublet) show no NOE contacts with either N-CH_2-Pr or Py-H3. The above NOE pattern is characteristic for the *mer*-coordination mode of a pyridine-amine-pyridine ligand, $PyCH_2$-N(CH_2R)-CH_2Py, clearly different from the NOE pattern characteristic for the *fac*-coordination mode (see ref 19).

(17) Due to the low yield of $\mathbf{6}^{2+}$ and $\mathbf{7}^+$, it was not possible to distinguish between their NMR signals that were generally overlapping with the signals of $\mathbf{5}^+$. For that reason the structure of $\mathbf{6}^{2+}$ with two CO ligands being *trans* to two picolyl donors and one *trans* to two amine donors is tentative, and it cannot be ruled out that the actual structure is similar to the structure of $\mathbf{2}^{2+}$, with one CO *trans* to two picolyl groups and two CO *trans* to one amine and one picolyl moiety.

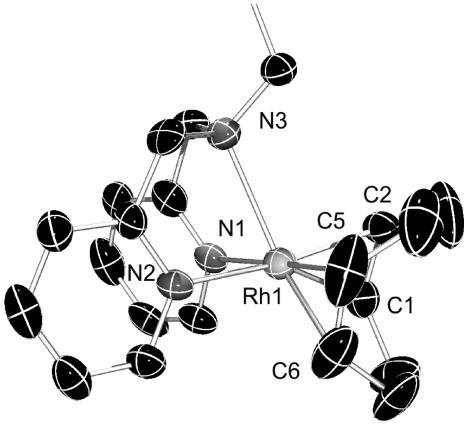

Figure 2. Coordination geometry of the rhodium atom in the complex $[Rh_2((\mu\text{-(bis-}\kappa^3\text{)tpen})_2(\eta^4\text{-cod})_2]^{2+}$ ($\mathbf{8}^{2+}$). Hydrogen atoms, the PF_6^- counterion, and the acetone molecule are omitted for clarity. Thermal ellipsoids are drawn with 50% probability. Selected bond lengths [Å] and angles [deg]: Rh1−C5 2.073(10); Rh1−C6 2.102(10); Rh1−C1 2.114(8); Rh1−N2 2.117(6); Rh1−C2 2.124(9); Rh1−N1 2.158(7); Rh1−N3 2.411(7); C1−C2 1.378(12); C5−C6 1.446(16); C5−Rh1−C6 40.5(4); C5−Rh1−C1 96.0(4); C6−Rh1−C1 79.9(4); C5−Rh1−N2 93.4(4); C6−Rh1−N2 90.0(3); C1−Rh1−N2 151.2(3); C5−Rh1−C2 81.1(5); C6−Rh1−C2 90.7(4); C1−Rh1−C2 38.0(3); N2−Rh1−C2 170.6(3); C5−Rh1−N1 175.5(4); C6−Rh1−N1 139.0(4); C1−Rh1−N1 88.0(3); N2−Rh1−N1 82.1(2); C2−Rh1−N1 103.4(4); C5−Rh1−N3 103.2(4); C6−Rh1−N3 141.1(4); C1−Rh1−N3 127.2(3); N2−Rh1−N3 76.3(2); C2−Rh1−N3 97.3(3); N1−Rh1−N3 75.7(3).

in methanol and precipitation as a PF_6^- salt. The N_3 ligand is coordinated in a *fac*-mode, and the cyclooctadiene is fluxional on the NMR time scale, which results in equivalent signals for both picolyl moieties and equivalent signals for the four olefinic protons of the cod fragment.

Crystals of $[\mathbf{8}](PF_6)_2$ suitable for X-ray diffraction were grown from acetone. The structure of $\mathbf{8}^{2+}$ is shown in Figures 2 and 3.

Significantly different bond distances between the rhodium atom and picolyl donors suggest a rather high distortion from the square-pyramidal geometry, with the weakest amine donor N3 being coordinated on the apical position. The bond distances are not significantly different from the bond distances of $[Rh_2(\kappa^3\text{-tpbn})(\eta^4\text{-cod})_2](PF_6)_2$ ($\mathbf{10}^{2+}$), partially caused by larger errors induced by some disorder in the crystal packing of the measured crystal of $\mathbf{8}^{2+}$.

Analysis of the X-ray structures of $[Rh_2((\mu\text{-(bis-}\kappa^3\text{)tpen})_2(\eta^4\text{-cod})_2]^{2+}$ ($\mathbf{8}^{2+}$) and $[Rh_2((\mu\text{-(bis-}\kappa^3\text{)tpbn})(\eta^4\text{-cod})_2]^{2+}$ ($\mathbf{10}^{2+}$) and DFT-optimized structure of $[Rh_2((\mu\text{-(bis-}\kappa^3\text{)tppn})(\eta^4\text{-cod})_2]^{2+}$[18] ($\mathbf{9}^{2+}$) indicates that the length of the methylene tether connecting bis(picolyl)amine moieties in tpbn, tppn, and tpen influences the structure of the binuclear complex. In the complexes with two or four carbon atoms in the tether, the two metal centers are found to be on the opposite sides of the molecule, in a "one hand up, one hand down" configuration. In complex $\mathbf{9}^{2+}$, having a C3 linker, the metal centers are on the same side, in a "hands up" configuration (see Figure 3).

These structural features of the tethered bpa-alkyl ligands proved to have an impact on the structure of corresponding rhodium carbonyl complexes (see below).

(18) X-ray structure of $[Rh_2(\kappa^3\text{-tppn})(\eta^4\text{-cod})_2](PF_6)_2$ has shown such connectivity; however very large disorder made the structure unsuitable for publication.

Dicationic complexes $[Rh_2((\mu\text{-(bis-}\kappa^3\text{)tpen})(CO)_2]^{2+}$ ($\mathbf{11}^{2+}$) and $[Rh_2((\mu\text{-(bis-}\kappa^3\text{)tppn})(CO)_2]^{2+}$ ($\mathbf{12}^{2+}$), dinuclear analogues of $\mathbf{5}^+$, were prepared by reaction of $[\{(CO)_2Rh(\mu\text{-Cl})\}_2]$ with the corresponding ligand in MeOH in a 1:1 molar ratio. Addition of NH_4PF_6 led to the precipitation of $\mathbf{11}^{2+}$ and $\mathbf{12}^{2+}$ as PF_6^- salts (Scheme 7). These complexes could also be prepared by treatment of $\mathbf{8}^{2+}$ or $\mathbf{9}^{2+}$ with 1 bar of CO.

In contrast to the reaction of $[\mathbf{5}]PF_6$, the reaction of $[\mathbf{12}](PF_6)_2$ in CH_3CN with 50 bar of CO is nearly quantitative within 4 days. The tetranuclear complex $[Rh_4((\mu\text{-CO})_3)_2((\mu\text{-(bis-}\kappa^3\text{)tppn})_2]^{4+}$, $[\mathbf{13}]^{4+}$, is formed, with two tris-μ-carbonyl bridges (Scheme 8). The $\nu_{(CO)}$ bands at 1838 and 1828 cm^{-1} (CH_3CN) and ^{13}C NMR triplets at $\delta = 215$ ($^1J_{C-Rh} = 29.1$ Hz) and $\delta = 213$ ($^1J_{C-Rh} = 29.1$ Hz) in approximate intensity ratio of 2:1 are indicative for the tris-μ-carbonyl bridges (Table 1). ^1H NMR and ^{13}C NMR signals for the tppn ligand show that $[\mathbf{13}]^{4+}$ has effective D_{2h} symmetry in solution (8 equivalent pyridyl fragments). The tppn ligand in $[\mathbf{13}]^{4+}$ is *fac*-coordinated, as indicated by ^1H-NOESY NMR.[19] For the DFT-optimized structure of $[\mathbf{13}]^{4+}$ see Supporting Information (Figure S1).

In contrast to $\mathbf{6}^{2+}$, $\mathbf{13}^{4+}$ is stable at room temperature both in the solid state and in solution. Heating $\mathbf{13}^{4+}$ in CH_3CN to 80 °C results in only approximately 20% conversion to $\mathbf{12}^{2+}$ in 2 h.

The stability of the tetranuclear complex $\mathbf{13}^{4+}$ is most likely a result of the cooperative binding of the four rhodium atoms through carbonyl bridges. Formation of the first Rh(μ-CO)$_3$Rh bridge (that is not thermodynamically stable for the binuclear analogue of $\mathbf{13}^{4+}$, the Bu-bpa complex $\mathbf{6}^{2+}$) enhances the effective local concentration of rhodium and entropically favors the formation of the second Rh(μ-CO)$_3$Rh bridge. This effect is similar to the well-known chelate effect that results in stronger binding of multidentate versus monodentate ligands. Consequently, multivalent binding (involving the interaction of four Rh atoms)[20] stabilizes $\mathbf{13}^{4+}$ from fragmentation into terminal Rh-CO complexes and results in higher stability of $\mathbf{13}^{4+}$ compared to $\mathbf{6}^{2+}$.

Under similar carbonylation conditions the tpen carbonyl complex $\mathbf{11}^{2+}$ (nor the tpen cod complex $\mathbf{8}^+$) did not form any bridged carbonyl species, and only $\mathbf{11}^{2+}$ could be observed in the solution. Although formation of an intramolecular CO bridge is not possible because of the "one hand up, one hand down'" conformation of the molecule, one could expect that intermolecular CO bridges could be formed, leading to polymeric structures. Formation of the CO-bridged species from the Bu-bpa complex $\mathbf{5}^+$ (for which the partial conversion to the bridged species $\mathbf{6}^{2+}$ was observed) and tpen complex $\mathbf{12}^{2+}$ would have approximately the same

(19) In $[(tppn)Rh_2(\mu_2\text{-CO})_3]^+$ ($[\mathbf{5}]^{4+}$) both the axial and the equatorial N-CH_2-Py protons (both AB-type doublets) show NOE contacts with Py-H3 and the β-CH_2 group of the propylene-diamine tether (N-CH_2-*CH_2*-CH_2-N). The α-CH_2 groups of the tether (N-*CH_2*-CH_2-*CH_2*-N) show only NOE contacts with the equatorial N-CH_2-Py protons (one of the two AB-type doublets) and not with the axial N-CH_2-Py protons. The above NOE pattern is characteristic for the *fac*-coordination mode of a pyridine-amine-pyridine ligand, $PyCH_2$-N(CH_2R)-CH_2Py, clearly different from the NOE pattern characteristic for the *mer*-coordination mode (see ref 16). The β-CH_2 group of the *n*-butylamine group in $[(BuBPA)Rh(cod)]^+$, $[\mathbf{1}]^+$, also shows NOE contacts with both the axial and the equatorial N-CH_2-Py protons. However, the observed exchange correlation (EXSY contact) between both N-CH_2-Py signals in $[\mathbf{1}]^+$ troubles further assignment of NOE contacts.

(20) (a) Mulder, A.; Huskens, J.; Reinhoudt, D. N. *Org. Biomol. Chem.* **2004**, *2*, 3409–3424. (b) Hunter, C. A.; Anderson, H. L. *Angew. Chem., Int. Ed.* **2009**, *48*, 7488–7499.

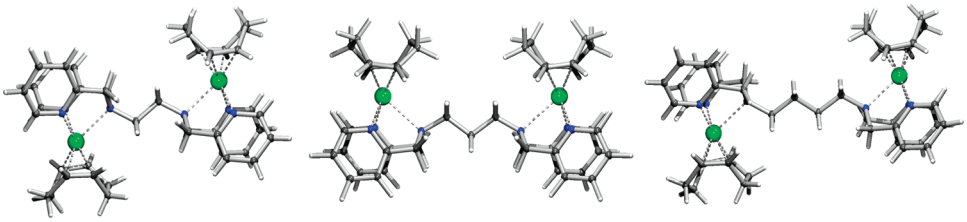

Figure 3. Molecular structures of $[Rh_2((\mu\text{-(bis-}\kappa^3\text{)tpen})_2(\eta^4\text{-cod})_2]^{2+}$ (**8**$^{2+}$), $[Rh_2((\mu\text{-(bis-}\kappa^3\text{)tppn})(\eta^4\text{-cod})_2]^{2+}$ (**9**$^{2+}$), and the previously reported $[Rh_2((\mu\text{-(bis-}\kappa^3\text{)tpbn})(\eta^4\text{-cod})_2]^{2+}$ (**10**$^{2+}$).

Scheme 7. Synthesis of Binuclear Rhodium Carbonyl Complexes $[Rh_2((\mu\text{-(bis-}\kappa^3\text{)tpen})(CO)_2]^{2+}$ ([11**]$^{2+}$) and $[Rh((\mu\text{-(bis-}\kappa^3\text{)tppn})(CO)_2]^{2+}$ ([**12**]$^{2+}$)**

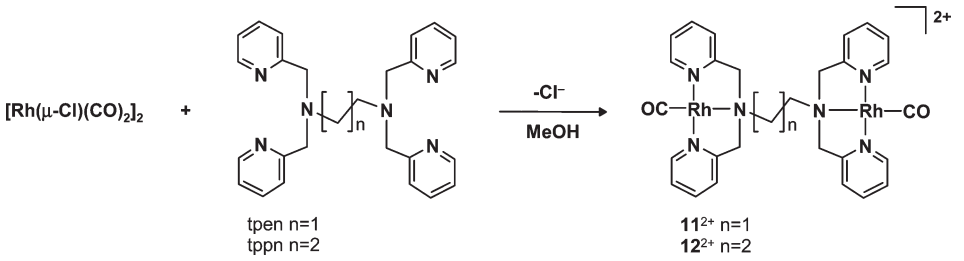

Scheme 8. Formation of Tetranuclear Rhodium Carbonyl Complex $[Rh_4((\mu\text{-CO})_3)_2(tppn)_2]^{4+}$, 13^{4+}

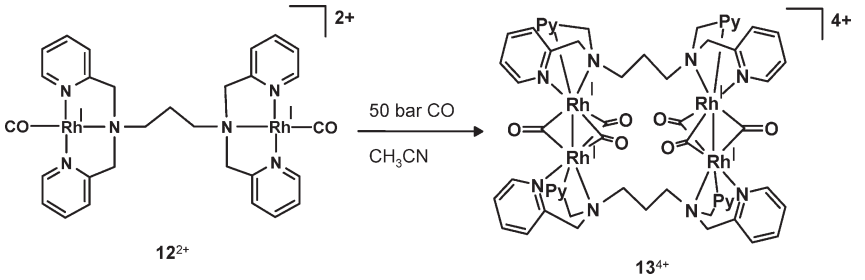

unfavorable entropy contribution, but the enthalpy of formation of the bridged species is likely even lower for tpen because of electronic effects. The tpen ligand imposes a lower electron density on the metal ($\nu_{(CO)}$ = 1999 cm^{-1}, $^1J_{C-Rh}$ = 67.5 Hz) compared to the Bu-bpa or tppn ligands ($\nu_{(CO)}$ = 1994 cm^{-1}, $^1J_{C-Rh}$ = 79 Hz) (Table 1), which most probably does not allow for coordination of any extra CO molecule. The lower donor capacity of the tpen ligand compared to Bu-bpa can be rationalized by the fact that the amine nitrogens of tpen are competing for the electrons from a very short C2 alkyl bridge, which effectively acts as an electron-poor "$CH_2^{\bullet}$ radical" substituent of the bpa moiety.

Treatment of the $[Rh_2((\mu\text{-(bis-}\kappa^3\text{)tpbn})(\eta^4\text{-cod})_2]^{2+}$ (**10**$^{2+}$) complex with 10 bar of CO at 50 °C for 10 h in acetonitrile results in formation of a yellow precipitate. IR measurements (KBr) showed the presence of bridging carbonyls ($\nu_{(CO)}$ = 1843 cm^{-1}) and a minor amount of terminal carbonyls ($\nu_{(CO)}$ = 1993 cm^{-1}) in the precipitate, while the filtrate after evaporation of the solvent gave signals at 1838 and 1992 cm^{-1}. This could indicate formation of polymeric $Rh(\mu\text{-CO})_3Rh$-bridged species, which should be driven by precipitation.

Rhodium Carbonyl Complexes with Tris(picolyl)amine. The above results suggest that the formation of the $Rh(\mu\text{-CO})_3$-Rh-bridged species is driven by use of stronger σ-donating N_3 ligands and can be further stabilized by entropic factors in the case of homoditopic ligands. To further investigate the effect of stronger σ-donors, we studied the tetradentate tpa (tpa = tris(picolyl)amine) ligand, which can be regarded as a bpa ligand functionalized with an additional picolyl group. This ligand can be compared with our previously reported Me_3tpa complexes in its coordinating behavior toward Rh-carbonyl species.[21]

Reaction of the *in situ* generated $[Rh(\mu\text{-Cl})(CO)_2]_2$ with tpa in methanol yields $[Rh(\kappa^3\text{-tpa})(CO)]PF_6$ ([**14**]PF_6) as a yellow powder after precipitation with KPF_6. Complexes **14**$^+$ with PF_6^-, B(*m*-xylyl)$_4^-$, and B(*m*-tolyl)$_4^-$ counterions (A^-) were also prepared by reaction of the $Rh(\kappa^3\text{-tpa})(ethene)^+(A^-)$ complexes with CO in the solid state. Solution IR in low concentration shows only one CO absorption band at 1991 cm^{-1}, indicating that the complex has a 16 VE square-planar geometry with the tpa ligand being in a κ^3-coordination mode. In polar solvents such as acetone or acetonitrile, the mononuclear species **14**$^+$ is in equilibrium with the dinuclear bis-μ-CO-bridged species $[Rh(\kappa^4\text{-tpa})(\mu\text{-CO})]_2^{2+}$ (**15**$^{2+}$) (Scheme 9), and at higher concentrations a weak IR absorption band at 1749 cm^{-1} reveals the formation of bridging ketonic carbonyls. After evaporation of the solvent a dark purple solid is obtained, showing an IR (solid state) absorption band of the bridging carbonyls of the dinuclear complex **15**$^{2+}$ at ν_{CO} = 1740 cm^{-1} and a terminal carbonyl band at 1985 cm^{-1} (Table 1). Formation of **15**$^{2+}$ is reversible, and dissolution of the solid purple mixture of **14**$^+$

(21) Dzik, W. I.; Smits, J. M. M.; Reek, J. N. H.; de Bruin, B. *Organometallics* **2009**, *28*, 1631–1643.

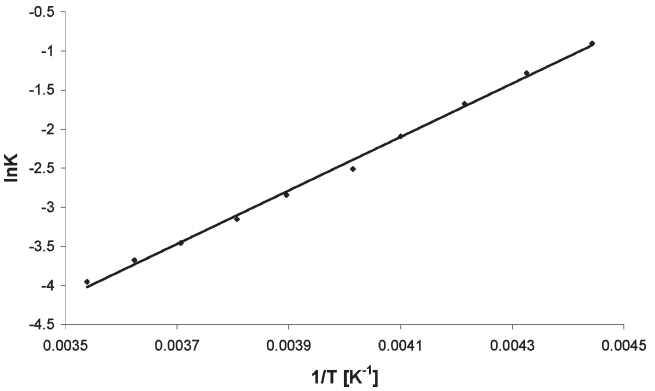

Figure 4. Van't Hoff plot of the dimerization of $\mathbf{14}^{+}$ to $\mathbf{15}^{2+}$: $\Delta H = -28.4 \pm 1.7$ kJ·mol^{-1}; $\Delta S = -134 \pm 7$ J·mol·K^{-1} ($r^2 = 0.9985$). The equilibrium constant is defined as $K = [\mathbf{15}^{2+}]/[\mathbf{14}^{+}]^2$.

Scheme 9. Dynamic Equilibrium between the Mononuclear $[Rh(\kappa^3\text{-tpa})(CO)]^{+}$ ($\mathbf{14}^{+}$) and Dinuclear $[Rh(\kappa^4\text{-tpa})(\mu\text{-CO})]_2^{2+}$ ($\mathbf{15}^{2+}$)

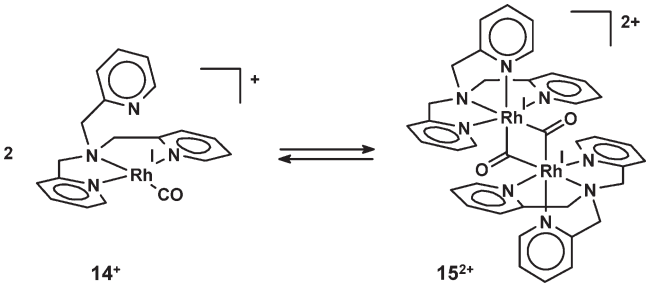

and $\mathbf{15}^{2+}$ leads to disappearance of the bridging carbonyl band. Such a monomer−dimer equilibrium is remarkable and has not been observed for the related $[Rh(\kappa^3\text{-Me}_3\text{tpa})(CO)]^{+}$ complex.[21] This different behavior should be ascribed to the stronger donor capacity of tpa versus Me_3tpa.

The equilibrium between the mononuclear and binuclear complexes could be studied by NMR in polar solvents such as acetonitrile or acetone, whereas in dichloromethane only the mononuclear form could be detected (see Figure S2, Supporting Information). Both the monomer and the dimer are fluxional on the NMR time scale, involving exchange of the axial and equatorial picolyl moieties. VT-NMR measurements further allowed us to calculate the thermodynamics for dimerization of $\mathbf{14}^{+}$ in acetone through a van't Hoff plot in the range from 283 to 225 K (Figure 4).

Formation of binuclear complex $\mathbf{15}^{2+}$ from $\mathbf{14}^{+}$ is enthalpically favorable by -28 kJ·mol^{-1}, but entropically disfavored. The large negative entropy factor of -134 J·mol·K^{-1} agrees well with a dimerization process and dominates at room temperature. The overall process at 298 K is slightly endergonic ($\Delta G^{\circ}_{298K} = +11.5$ kJ·mol^{-1}, $K_{298K} \approx 9.5 \times 10^{-3}$).

The ^{1}H NMR spectra recorded in the temperature range from 330 to 218 K are presented in Figure 5. At 330 K only the mononuclear form $\mathbf{14}^{+}$ is visible ($K_{330K} \approx 3.2 \times 10^{-3}$). All the picolyl arms of the ligand are equivalent, which indicates that at this temperature the molecule is fluxional on the NMR time scale. This process is frozen at 263 K, where the protons of the coordinated and dangling picolyl groups show different signals. We expect that the mechanism of fluxionality of $\mathbf{14}^{+}$ is the same as for the recently reported $[Rh(Me_3tpa)CO]^{+}$; that is, the dangling picolyl arm coordinates

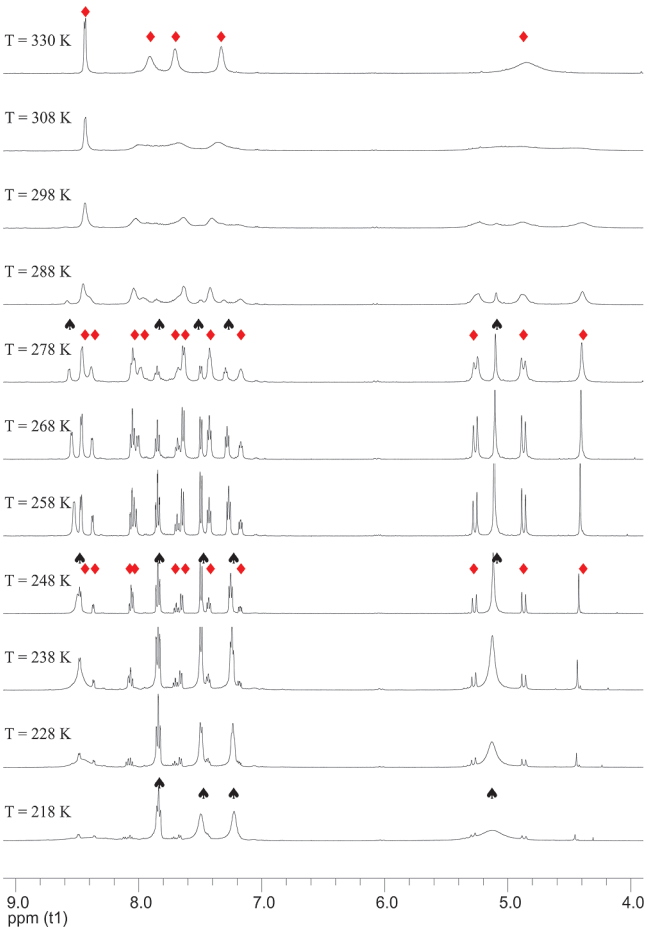

Figure 5. Variable-temperature ^{1}H NMR spectrum showing dimerization of $\mathbf{14}^{+}$ and the fluxional behavior of $\mathbf{14}^{+}$ and $\mathbf{15}^{2+}$ in acetone-d_6. Legend: red points = $\mathbf{14}^{+}$; black points = $\mathbf{15}^{2+}$.

to the metal, forming a transient 18 VE κ^4-complex followed by dissociation of another picolyl moiety to re-form the 16 VE square-planar κ^3-complex.[21]

The signals of the dinuclear species $\mathbf{15}^{2+}$ start to appear upon cooling the solution close to room temperature. The signals of both the mononuclear species $\mathbf{14}^{+}$ and dinuclear species $\mathbf{15}^{2+}$ are substantially broadened at 308 K. Sharpening of the signals of both compounds appears in the same temperature range. This behavior indicates that the broadening is due to coalescence associated with the reversible dimerization of $\mathbf{14}^{+}$ to $\mathbf{15}^{2+}$. The signals of all three picolyl arms of the dinuclear compound $\mathbf{15}^{2+}$ are equivalent down to 218 K. Clearly the dinuclear complex remains fluxional in the entire measured temperature range. At temperatures below 253 K the signals of the dimer are becoming broader and the signal of Py-H6 completely disappears at 218 K while approaching coalescence.[22]

Since the fluxional behavior of $\mathbf{15}^{2+}$ down to 218 K is not caused by the dimer−monomer equilibrium, it has to originate from exchange of the picolyl moieties on the octahedral 18 VE rhodium center that is fast on the NMR time scale. Noticeably, the octahedral 18 VE complex $\mathbf{2}^{2+}$ does not show a similar fluxional behavior in solution. An important difference between $\mathbf{2}^{2+}$ and $\mathbf{15}^{2+}$ is the presence of a Rh−Rh bond in the former, which is absent in the latter (see below).

(22) Unfortunately, we were not able to record spectra below 218 K because of the NMR spectrometer restrictions.

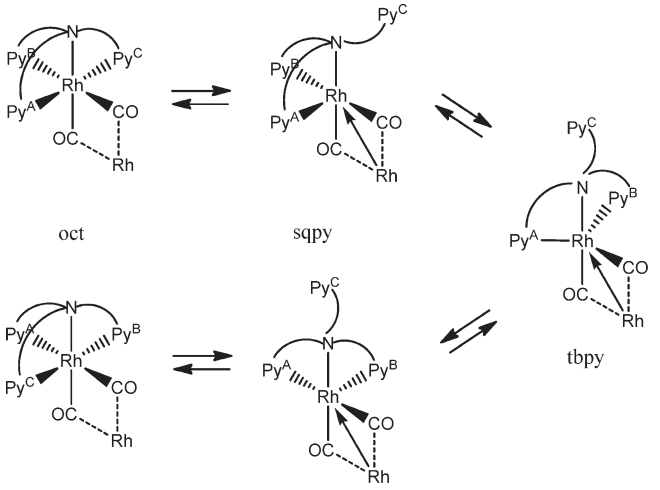

Figure 6. Proposed mechanism of exchange of the pyridyl groups of $\mathbf{15}^{2+}$ leading to observed fluxionality of the complex.

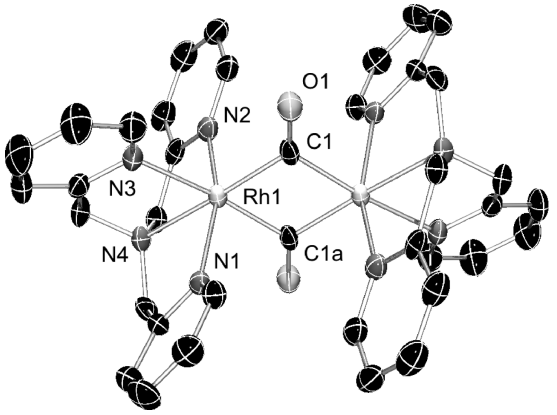

Figure 7. X-ray structure of $[Rh(\kappa^4\text{-tpa})(\mu\text{-CO})]_2^{2+}$, $\mathbf{15}^{2+}$. Thermal ellipsoids are drawn with 50% probability. Hydrogen atoms, the B(*p*-tolyl)$_4^-$ counterions, and two dichloromethane molecules are omitted for clarity. Selected bond lengths [Å] and angles [deg]: Rh1−C1 1.972(4), Rh1−C1a 1.993(4), Rh1−N2 2.088(3), Rh1−N1 2.111(3), Rh1−N4 2.201(3), Rh1−N3 2.242(3), C1−O1 1.205(5), N1−Rh1−N4 80.14(12), N1−Rh1−N3 81.07(12), N2−Rh1−N4 79.13(12), N2−Rh1−N3 93.62(12), C1−Rh1−C1a 79.05(18).

We therefore propose that the exchange process of $\mathbf{15}^{2+}$ follows the sequence shown in Figure 6. Decoordination of one of the picolyl arms (Py^C *trans* to Py^A) leads to a transient 16 VE square-pyramidal species that can rearrange the coordinated picolyl groups via a Berry-preudorotation mechanism (via a trigonal-bypiramidal structure). Recoordination of the free picolyl group leads to re-formation of the octahedral species with a different order of the picolyl groups. DFT calculations suggest that the detachment of the picolyl moiety of $\mathbf{15}^{2+}$ is facilitated by formation of a weak σ-type metal−metal interaction in the "unsaturated" tbpy intermediate (see Supporting Information, Figure S3). Compound $\mathbf{2}^{2+}$ already has a σ-type Rh−Rh bond and cannot easily increase its bond order, and hence the pentacoordinate intermediate required for exchange should be less easily accessible.

Formation of the dinuclear species $\mathbf{15}^{2+}$ was further confirmed by single-crystal X-ray diffraction. Top layering a dichloromethane solution of [**14**](B(*m*-tolyl)$_4$)$_2$ with hexanes yielded purple crystals of [**15**](B(*m*-tolyl)$_4$)$_2$. The molecular structure of $\mathbf{15}^{2+}$ is shown in Figure 7.

Scheme 10. Reaction of $[Rh(\kappa^3\text{-tpa})(CO)]^+$ ($\mathbf{14}^+$) with Dioxygen to Form the Carbonato Complex $[Rh(\kappa^4\text{-tpa})(CO)_3]^+$ ($\mathbf{16}^+$)

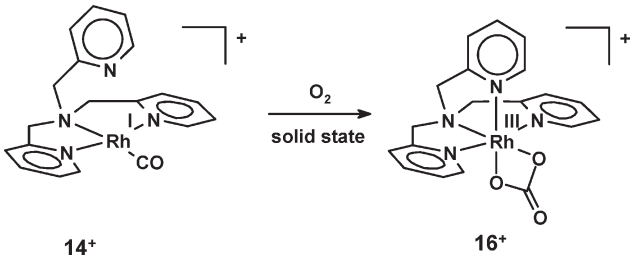

The Rh−Rh distance of 3.0585(7) indicates little or no bonding interaction between the metal atoms,[23] in agreement with the saturated 18 VE configuration of the two metals in the absence of a Rh−Rh bond. The Rh−C−Rh angle (100.9(2)°) is considerably larger than the usual 80−90° bond of the "classical" bridging rhodium carbonyls.[24] Although the angle is somewhat more acute than most of the reported M−C−M angles for ketonic carbonyls (having more sp^2 character of the carbon atom), which are in the range 107−120°,[25] the CO stretching frequency of 1749 cm^{-1} (MeCN) is in full agreement with a ketonic character of the carbonyl group.[25d,e] To our best knowledge, complex $\mathbf{15}^{2+}$ is the first example of a binuclear bis-CO-bridged rhodium species not supported by any other ancillary bridging ligands, nor a Rh−Rh bond.[26] This seems to be also the first example of a dynamic equilibrium between a mononuclear terminal carbonyl Rh^I species and binuclear $Rh(\mu\text{-CO})_xRh$-bridged species measured in solution.

In the solid state $\mathbf{14}^+$ reacts with air to form carbonato complex $[Rh(\kappa^4\text{-tpa})(CO_3)]^+$ ($\mathbf{16}^+$), similar to the oxygenation reaction recently reported for $[Rh(\kappa^3\text{-Me}_3\text{tpa})(CO)]^+$[21] (Scheme 10). Reaction with air in dichloromethane or acetone/water led to a mixture of unidentified products. Top layering a dichloromethane solution of [**16**]B(*m*-xylyl)$_4$ with hexanes yielded crystals of [**16**]B(*m*-xylyl)$_4$ suitable for X-ray diffraction (Figure 8).

As expected, the Rh−N bond distances of $\mathbf{16}^+$ are considerably shorter than in the analogous complex $[Rh(Me_3tpa)(CO_3)]^+$, in which the ligand tpa is functionalized with methyl groups on the 6 position of the pyridyl ring.[21]

The structure of $\mathbf{16}^+$ is similar to the structure of $[Co(tpa)(CO_3)]^+$,[27] albeit with longer metal to ligand bonds.

(23) The longest reported unsupported Rh−Rh bonds do not exceed 2.93−2.94 Å: Chifotides, H. T. Dunbar, K. R. In *Multiple Bonds between Metal Atoms*, 3rd ed.; Cotton, F. A.; Murillo, C. A.; Walton, R. A., Eds.; Springer: New York, 2005; pp 465−589, and references therein.

(24) Colton, R.; McCormick, M. J. *Coord. Chem. Rev.* **1980**, *31*, 1–52.

(25) For examples see: (a) Cowie, M.; Southern, T. G. *Inorg. Chem.* **1982**, *21*, 246–253. (b) Cowie, M.; Vasapollo, G.; Sutherland, B. R.; Ennett, J. P. *Inorg. Chem.* **1986**, *25*, 2648–2653. (c) Carmona, D.; Ferrer, J.; Lahoz, F. J.; Oro, L. A.; Reyes, J.; Esteban, M. *J. Chem. Soc., Dalton Trans.* **1991**, 2811–2820. (d) Connelly, N. G.; Einig, T.; Herbosa, G. G.; Hopkins, P. M.; Mealli, C.; Orpen, A. G.; Rosair, G. M.; Viguri, F. *J. Chem. Soc., Dalton Trans.* **1994**, 2025–2039. (e) Tejel, C.; Bordonaba, M.; Ciriano, M. A.; Edwards, A. J.; Clegg, W.; Lahoz, F. J.; Oro, L. A. *Inorg. Chem.* **1999**, *38*, 1108–1117.

(26) Crystal structures of bis-μ-CO-bridged rhodium species supported by a Rh−Rh bond: (a) Allevi, C.; Golding, M.; Heaton, B.; Ghilardi, C. A.; Midollini, S.; Orlandini, A. *J. Organomet. Chem.* **1987**, *326*, C19–C22. (b) Enders, M.; Kohl, G.; Pritzkow, H. *J. Organomet. Chem.* **2004**, *689*, 3024–3030. Similar tetranuclear species were also reported: (c) Lahoz, F. J.; Martin, A.; Estruelas, M. A.; Sola, E.; Serrano, J. L.; Oro, L. A. *Organometallics* **1991**, *10*, 1794–1799. (d) Cotton, F. A.; Dikarev, E. V.; Petrukhina, M. A. *J. Chem. Soc., Dalton Trans.* **2000**, 4241–4243.

(27) Cheyne, S. E.; McClintock, L. F.; Blackman, A. G. *Inorg. Chem.* **2006**, *45*, 2610–2618.

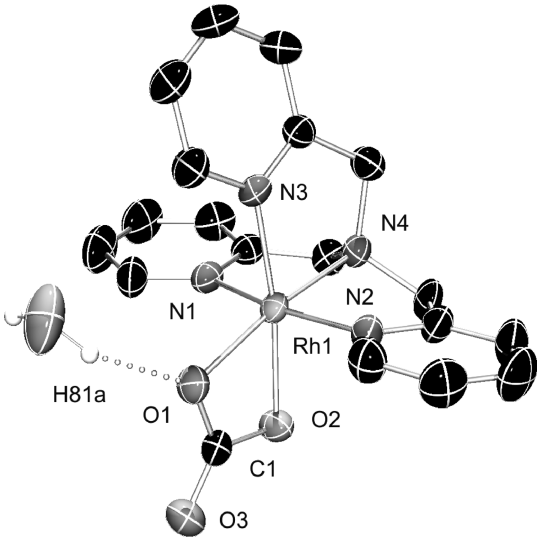

Figure 8. X-ray structure of $[Rh(\kappa^4\text{-tpa})(CO)_3]^+ \cdot H_2O$ ($\mathbf{16}^+ \cdot H_2O$). Thermal ellipsoids are drawn with 50% probability. Hydrogen atoms of the tpa ligand and the B(*m*-xylyl)$_4^-$ counterion were omitted for clarity. Selected bond lengths [Å] and angles [deg]: Rh1−N3 2.007(3), Rh1−N2 2.012(3), Rh1−O2 2.021(2), Rh1−N4 2.030(3), Rh1−N1 2.033(3), Rh1−O1 2.036(2), Rh1−C1 2.462(4), C1−O3 1.224(4), C1−O1 1.318(4), C1−O2 1.334(4), H81a−O1 1.94(4); O2−Rh1−N4 106.15(10), O2−Rh1−N2 88.95(11), N4−Rh1−N2 82.77(11), O2−Rh1−O1 65.11(9), N4−Rh1−O1 171.23(10), N2−Rh1−O1 95.97(10), O2−Rh1−N3 171.01(10), N4−Rh1−N3 82.45(10), N2−Rh1−N3 94.85(11), O1−Rh1−N3 106.32(10), O2−Rh1−N1 91.49(10), N4−Rh1−N1 84.34(11), N2−Rh1−N1 166.69(11), O1−Rh1−N1 96.28(11), N3−Rh1−N1 86.68(11).

Although the picolyl moiety is a stronger donor than amine, the Rh−O1 bond *trans* to the amine N4 is slightly longer compared with the Rh−O2 bond *trans* to the picolyl N3. This is most probably caused by the hydrogen bonding between O1 and a water molecule present in the unit cell.

Conclusions

Synthesis of rhodium carbonyl complexes ligated with a series of different bis(2-picolyl)amine derivatives allowed us to study the factors that determine the relative stabilities of terminal monocarbonyl and tris-carbonyl bridges. Whereas for the relatively strong electron-donating bpa ligand the formation of the $Rh(\mu\text{-}CO)_3Rh$ bridge is thermodynamically favorable at 1 bar of CO, weaker donors such as Bu-bpa or tpen do not allow formation of such species under such conditions. The unfavorable entropy of formation of the carbonyl bridges can be reduced by tethering the bpa moieties with a propylene linker. This allows for cooperative binding of four rhodium centers to assemble a stable tetranuclear compound with two tris-carbonyl bridges.

Similarly, the stronger tris(2-picolyl)amine (tpa) N_4 donor allows formation of ketonic bis-carbonyl-bridged species $\mathbf{15}^{2+}$, which exists in dynamic equilibrium with the mononuclear monocarbonyl species $\mathbf{14}^+$ in solution, whereas Rh-carbonyl species with the weaker N_4-donor Me_3tpa (tris(2,6-lutidyl)-amine) exist only in the mononuclear terminal carbonyl form. We thus showed that subtle changes in the ligand structure have a major impact on the stability of the carbonyl-bridged compounds compared to their terminal monocarbonyl analogues. The presented results clearly show that the stability of the bis- and tris-carbonyl-bridged structures depends on a delicate balance between favorable enthalpic factors (enhanced with stronger σ-donor ligands) and unfavorable entropic factors (that can be reduced by multinuclear binding using ditopic ligands).

Experimental Section

General Methods. All procedures were performed under N_2 using standard Schlenk techniques. Solvents (p.a.) were deoxygenated by bubbling through a stream of N_2 or by the freeze−pump−thaw method. The temperature indication rt corresponds to ca. 20 °C. $[\{(CO)_2Rh(\mu\text{-}Cl)\}_2]$,[28] tppn,[29] $[Rh(\kappa^3\text{-bpa})(\eta^4\text{-cod})]PF_6$ ($[\mathbf{1}]PF_6$), $[Rh(\kappa^3\text{-Bu-bpa})(\eta^4\text{-cod})]PF_6$ ($[\mathbf{4}]PF_6$), and $[Rh_2((\mu\text{-(bis-}\kappa^3)\text{tpbn})(\eta^4\text{-cod})_2](PF_6)_2$ ($[\mathbf{10}](PF_6)_2$)[11] were prepared according to literature procedures. All other chemicals are commercially available and were used without further purification.

NMR experiments were carried out on a Bruker DPX200 (200 and 50 MHz for ^1H and ^{13}C, respectively), Bruker AC300 or DRX300 (300 and 75 MHz for ^1H and ^{13}C, respectively), Bruker WM400 (400 and 100 MHz for ^1H and ^{13}C, respectively), and Varian Inova500 (500 and 125 MHz for ^1H and ^{13}C, respectively). Solvent shift reference for ^1H NMR: [D$_6$]-acetone δ_H = 2.05, CD_3CN δ_H = 1.98. For ^{13}C NMR: [D$_6$]-acetone δ_C = 29.50, CD_3CN δ_C = 1.28. Abbreviations used are s = singlet, d = doublet, dd = doublet of doublets, t = triplet, p = pentet, m = multiplet, and br = broad. The couplings between the protons in the pyridine ring are not fully resolved, and hence we use a simplified assignment of the multiplicities of the signals as doublets, triplets, and double triplets.

Elemental analyses (C, H, N) were carried out on a Carlo Erba NCSO-analyzer. Mass spectra (FAB) were recorded on a VG 7070 mass spectrometer or on a JEOL JMS SX/SX102A four-sector mass spectrometer. Solution and KBr FT-IR spectra were recorded on a Perkin-Elmer 1720X spectrometer or on a Bruker Vertex 70 FTIR spectrometer. Solid-state IR measurements were performed on a Shimadzu FTIR 8400S spectrometer equipped with a Specac MKII Golden Gate Single Reflection ATR system.

X-ray Diffraction. The structures are shown in Figures 1, 2, 7, and 8,[30] which include selected bond distances and angles. The crystal data are shown in Table 2. Crystals were mounted on glass needles. The intensity data of $[\mathbf{2}](PF_6)_2$, $[\mathbf{15}](B(p\text{-tolyl})_4)_2$, and $[\mathbf{16}]B(m\text{-xylyl})_4$ were collected on a Nonius Kappa CCD single-crystal diffractometer, using Mo Kα radiation and applying ϕ and ω scan modes. The intensity data of $[\mathbf{8}](PF_6)_2$ were collected on an Enraf-Nonius CAD4 single-crystal diffractometer using Mo Kα radiation and applying the ω scan mode. The intensity data were corrected for Lorentz and polarization effects. A semiempirical multiscan absorption correction was applied (SADABS)[31] on [**2**], [**15**], and [**16**], while [**8**] was corrected for absorption semiempirically from ψ scans. The structures were solved by the PATTY option[32] of the DIRDIF program system.[33] All non-hydrogen

(28) McCleverty, J. A.; Wilkinson, G.; Lipson, L. G.; Maddox, M. L.; Kaesz, H. D. *Inorg. Synth.* **1990**, *28*, 84.
(29) tppn has been prepared by a method similar to that reported for tpen: Toftlund, H.; Yde-Andersen, S. *Acta Chem. Scand., Ser. A* **1981**, *35*, 575–585.
(30) (a) Ortep-3 for Windows: Farrugia, L. J. *J. Appl. Crystallogr.* **1997**, *30*, 565. (b) Rendering was made with POV-Ray 3.6, Persistence of Vision Pty. Ltd. (2004), Persistence of Vision Raytracer (Version 3.6), retrieved from http://www.povray.org/download/.
(31) Sheldrick, G. M. *SADABS*; University of Göttingen: Germany, 1996.
(32) Beurskens, P. T.; Beurskens, G.; Strumpel, M.; Nordman, C. E. In *Patterson and Pattersons*; Clarendon: Oxford, 1987; p 356.
(33) Beurskens, P. T.; Beurskens, G.; Bosman, W. P.; de Gelder, R.; García-Granda, S.; Gould, R. O.; Israël, R.; Smits, J. M. M. *DIRDIF program system*; University of Nijmegen: The Netherlands, 1996.

Table 2. Crystallographic Data for [2](PF$_6$)$_2$, [8](PF$_6$)$_2$, [15](B(*p*-tolyl)$_4$)$_2$, and [16]B(*m*-xylyl)$_4$

	$[Rh_2(\kappa^3\text{-bpa})_2(\mu\text{-}CO)_3](PF_6)_2\cdot 2C_3H_6O$	$[Rh_2((\mu\text{-(bis-}\kappa^3)\text{tpen})(\eta^4\text{-cod})_2](PF_6)_2\cdot C_3H_6O$	$[Rh(tpa)CO]_2(B\text{-tolyl}_4)_2\cdot 4CH_2Cl_2$	$[Rh(tpa)(CO_3)](B\text{-xylyl}_4)\cdot H_2O$
cryst color	translucent yellow-green	translucent yellow	dark brown	translucent light yellow
cryst shape	rather regular rod	irregular chunk	rough rod	rough fragment
cryst size [mm]	0.28 × 0.14 × 0.13	0.35 × 0.19 × 0.10	0.72 × 0.24 × 0.13	0.28 × 0.24 × 0.22
empirical formula	$C_{33}H_{38}F_9N_6O_5P_{1.50}Rh_2$	$C_{24}H_{32}F_6N_3OPRh$	$C_{98}H_{100}B_2Cl_8N_8O_2Rh_2$	$C_{51}H_{56}BN_4O_4Rh$
fw	1021.97	626.41	1932.90	902.72
temperature [K]	208(2)	298(2)	208(2)	298(2)
radiation	Mo Kα (graphite mon.)	Mo Kα (graphite mon.)	Mo Kα (graphite mon.)	Mo Kα (graphite mon.)
wavelength [Å]	0.71073	0.71073	0.71073	0.71073
cryst syst	tetragonal	monoclinic	triclinic	monoclinic
space group	$I\bar{4}2d$	$P2_1/n$	$P\bar{1}$	$P2_1/n$
a [Å]	30.368(8)	9.3568(9)	13.8374(10)	9.9552(9)
b [Å]	30.368(8)	21.675(2)	14.319(2)	24.1566(7)
c [Å]	9.2873(4)	13.0980(14)	14.5273(9)	21.377(2)
α [deg]	90	90	115.639(7)	90
β [deg]	90	92.54(2)	111.926(7)	96.852(8)
γ [deg]	90	90	94.289(10)	90
volume [Å]	8565(3)	2653.7(5)	2309.1(4)	5104.2(7)
Z	8	4	1	4
density [Mg m^{-3}]	1.585	1.568	1.390	1.175
abs coeff [mm^{-1}]	0.910	0.768	0.642	0.378
diffractometer	Nonius KappaCCD with area detector	Enraf-Nonius CAD4	Nonius KappaCCD with area detector	Nonius KappaCCD with area detector
scan	ϕ and ω scan	ω scan	ϕ and ω scan	ϕ and ω scan
F(000)	4092	1276	996	1888
θ range [deg]	2.12 to 25.00	1.82 to 24.97	2.14 to 25.00	3.00 to 27.50
index ranges	$-36 \le h \le 36$ $-36 \le k \le 36$ $-11 \le l \le 11$	$0 \le h \le 11$ $-25 \le k \le 25$ $-15 \le l \le 15$	$-16 \le h \le 16$ $-17 \le k \le 17$ $-17 \le l \le 17$	$-12 \le h \le 12$ $-31 \le k \le 31$ $-26 \le l \le 27$
reflns collected/ unique	82 568/3781	9730/4648	25 089/8074	98 373/11 680
R(int)	0.1218	0.1070	0.0573	0.0586
reflns obsd [$I_o > 2\sigma(I_o)$]	3738	2478	6527	8901
data/restraints/ params	3781/0/261	4648/3/338	8074/0/545	11 680/2/564
goodness-of-fit on F^2	1.231	1.021	1.052	1.107
SHELXL-97 weight params	0.0732, 193.7360	0.0687, 0.6537	0.0379, 4.2236	0.0628, 3.9564
final R indices [$I > 2\sigma(I)$]				
R_1	0.0877	0.0688	0.0485	0.0580
wR_2	0.2183	0.1375	0.1005	0.1282
R indices (all data)				
R_1	0.0883	0.1516	0.0714	0.0896
wR_2	0.2187	0.1683	0.1101	0.1393
largest diff peak and hole [e·Å^{-3}]	1.681/−1.116	0.634/−0.543	0.692/−0.635	1.073/−0.329

atoms were refined with anisotropic temperature factors. The hydrogen atoms were placed at calculated positions and refined isotropically in riding mode, except for the hydrogen atoms on O81 in [**16**]B(*m*-xylyl)$_4$, which were refined freely.

[2](PF$_6$)$_2$. The crystal structure analysis was hampered by PF$_6$ disorder and the poor quality of the data. Because of the limited reliability of the higher order data, all data above 25° θ were not used in the refinement. The least-squares refinement showed a moderate racemic twinning (BASF = 0.113). The difference Fourier map showed a substantial residual density, which could not be parametrized, and therefore the SQUEEZE procedure[34] was used to account for this electron density. Nevertheless the final difference Fourier map showed rather large residual density, especially close to the rhodium atom. To a large extent this is probably due to absorption effects.

The parameter set suggests a ratio of 1 dinuclear Rh complex:1.5 PF$_6$ moieties:2 acetone moieties. Obviously, the correct charge balance of the dinuclear Rh complex (as confirmed by the analytical and spectroscopic data of [**2**](PF$_6$)$_2$, see Synthesis section below) requires the presence of 2 PF$_6$ moieties per complex; therefore we have to assume that the residual electron density stands for 0.5 PF$_6$ (4 PF$_6$ moieties in the whole unit cell). The SQUEEZE procedure shows four voids of 229 Å^3 each, containing 52 electrons in the whole unit cell. These voids are centered around positions with $y = 0.25$ and $y = 0.75$, so around special positions with a multiplicity of 4, which is in accord with the number of missing PF$_6$ moieties. The number of electrons in these voids reported by the SQUEEZE procedure (52/void) is rather low, as a PF$_6$ moiety has 69 electrons. However, the voids are rather large and therefore merge to form channels through the structure running parallel to the *c*-axis. Measurements on crystals grown from acetone/diethyl ether did not result in improved data; indeed they were worse. However, these data showed indications of the missing PF$_6$ moieties on a general position in these channels, in which case an occupancy factor of 0.5 has to be assumed, together with the presence of more, unidentified solvent moiety (acetone or diethyl ether). Despite the problems encountered with this structure, we do believe that the structure and geometry of the dicationic dinuclear Rh complex are correct and reliable. The physical properties given here are based on the presence of 2 PF$_6$ and 2 acetone moieties in the structure.

(34) Spek, A. L. *PLATON, A Multipurpose Crystallographic Tool*; Utrecht University: Utrecht, The Netherlands, 2003.

[8](PF$_6$)$_2$. The PF_6 moiety is rather disordered, as is the acetone moiety (C_3H_6O). Within the acetone moiety only atom C43 could be split up during the refinement, but all C−C bond distances had to be restrained. It was not possible to parametrize the PF_6 disorder. The same holds for the acetone. Moreover, it is unlikely that the acetone parameters give an adequate description of the disorder: the geometry of at least one of the two proposed positions is unsatisfactory, but based on the synthetic route and packing considerations acetone seems to be the only likely candidate for the electron density present in the Fourier map. Geometrical calculations[34] revealed neither unusual geometric features nor unusual short intermolecular contacts. The calculations revealed no higher symmetry and no (further) solvent-accessible areas.

[15](B(*p*-tolyl)$_4$)$_2$. Only one suitable, rather fragile, single crystal was available, and therefore it was not cut to a smaller size. A collimator producing an X-ray beam of 0.8 mm was used during the measurements. Geometrical calculations revealed neither unusual geometric features nor unusual short intermolecular contacts. The calculations revealed no higher symmetry and no (further) solvent-accessible areas.

[16](B(*m*-xylyl)$_4$). The hydrogen atoms, except those on O81, were placed at calculated positions and refined isotropically in riding mode. The hydrogen atoms on O81 were found from a difference Fourier map, but the O−H bond distances had to be restrained in order to prevent physically unacceptable results.

The structure contains some heavily disordered and probably partially occupied solvent moieties. Attempts to parametrize these moieties were not successful and resulted in physically unacceptable results or unstable refinements.

Therefore the SQUEEZE procedure[34] was used to account for the observed electron density. It detected two symmetry-related voids of 367 Å^3 containing 11 electrons each. This electron count is not very likely, and therefore we assume partial occupancy. It is not possible to draw any reliable conclusions about the nature of the moieties or the amount present, and hence they could not be taken into account while calculating physical properties. Geometrical calculations revealed neither unusual geometric features nor unusual short intermolecular contacts. The calculations revealed no higher symmetry and no (further) solvent-accessible areas.

DFT Calculations. Geometry optimizations were carried out with the Turbomole program package[35] coupled to the PQS Baker optimizer[36] at the ri-DFT[37] level using the BP86[38] functional and SV(P) basis set.[39]

Measurements of the Equilibrium between 14^+ and 15^{2+}. Measurements were performed on a 0.0036 M solution of $\mathbf{14}^+$ in acetone-d_6 on a Bruker DRX300 NMR spectrometer. The sample temperature was calibrated by measuring the chemical-shift separation between the OH and CH_3 resonances of methanol. Relative concentrations of $\mathbf{14}^+$ and $\mathbf{15}^{2+}$ were estimated by integration of the $-CH_2-$ proton signals of the tpa ligand.

Synthesis. [Rh$_2$(κ^3-bpa)$_2$(μ-CO)$_3$](PF$_6$)$_2$ ([2](PF$_6$)$_2$). A 290 mg portion of [Rh(bpa)(cod)]PF_6 (0.522 mmol) was placed in a 100 mL Schlenk flask and dissolved in 15 mL of CH_2Cl_2. CO was bubbled through the solution for 25 min, during which a yellow precipitate formed. The solution was stirred for an additional 30 min under CO atmosphere, and the yellow solid was filtered and dried *in vacuo*. Yield: 167 mg (0.170 mmol, 65.4%). ^{1}H NMR (500 MHz, CD_3CN): δ 8.62 (d, ^3J(H,H) = 4.5 Hz, 1H; Py-H6); 8.52 (d, ^3J(H,H) = 4.5 Hz, 1H; Py-H6′); 7.88 (dt, ^4J(H,H) = 1.5 Hz, ^3J(H,H) = 8.0 Hz, 2H; Py); 7.46 (m, 3H; Py); 7.38 (t, ^3J(H,H) = 6.0 Hz, 1H; Py); 5.72 (t, ^3J(H,H) = 4.0 Hz, 1H; NH); 4.87 (dd[AB], ^2J(H,H) = 17.0 Hz, ^3J(H,H) = 7.0 Hz, 2H; N−CH_2-Py); 4.78 (dd[AB], ^2J(H,H) = 17.0 Hz, ^3J(H,H) = 7.0 Hz, 2H; N-CH_2-Py); 4.33 (m, 4H; N-CH_2-Py). ^{13}C NMR (125 MHz, CD_3CN): δ 215.8 (t, ^1J(C,Rh) = 28.4 Hz, 2xμ_2-CO), 210.4 (t, ^1J(C,Rh) = 27.9 Hz, μ_2-CO); 161.1 (Py-C1); 160.9 (Py-C1′); 149.5 (Py-C5); 149.3 (Py-C5′); 140.8 (Py-C3); 140.7 (Py-C3′); 125.8 (Py); 124.8 (Py); 60.0 (N-CH_2-Py); 59.9 (N-CH_2-Py′). IR (MeCN): $\nu_{(C\equiv O)}$ = 1835 with a shoulder at 1828 cm^{-1}, solid state: $\nu_{(C\equiv O)}$ = 1836, 1815 cm^{-1}. Anal. Calcd ($C_{27}H_{26}F_{12}N_6O_3P_2Rh_2\cdot 0.5CH_2Cl_2$): C, 32.36; H, 2.67; N, 8.23. Found: C, 32.34; H, 2.97; N, 8.43.

[Rh(κ^3-bpa)(CO)]PF$_6$ ([3]PF$_6$). A 153 mg amount of [2](PF$_6$)$_2$ (0.156 mmol) was dissolved in 10 mL of MeOH and kept under reflux for 3 h, allowing the evolved CO to escape from the vessel. The unreacted [2](PF$_6$)$_2$ was filtered off, and the filtrate was condensed to ca. 5 mL, causing precipitation of the product, which was filtered off and dried *in vacuo*. Yield: 59 mg (0.124 mmol, 39.6%). ^{1}H NMR (300 MHz, CD_3CN): δ 8.39 (d, ^3J(H,H) = 5.4 Hz, 2H; Py); 7.92 (dt, ^4J(H,H) = 1.5 Hz, ^3J(H,H) = 7.8 Hz, 2H; Py); 7.34 (d, ^3J(H,H) = 8.1 Hz, 2H; Py); 7.30 (t, ^3J(H,H) = 6.9 Hz, 2H; Py); 5.57 (s, br, 1H, N-H); 4.60 (d[AB], ^2J(H,H) = 15.9 Hz, ^3J(H,H) = 9.6 Hz, 2H; N-CH_2-Py); 4.46 (d[AB], ^2J(H,H) = 15.9 Hz, ^3J(H,H) = 6.0 Hz, 2H; N-CH_2-Py). ^{13}C NMR (75 MHz, CD_3CN): δ 190.3 (d, ^1J(Rh,C) = 77.5 Hz; (CO)); 165.2 (Py); 154.6 (Py); 139.8 (Py); 125.7 (Py); 123.4 (Py); 57.8 (N-CH_2-Py). IR (MeCN): $\nu_{(C\equiv O)}$ = 1989 cm^{-1}. Anal. Calcd ($C_{13}H_{13}F_6N_3OPRh$): C, 32.86; H, 2.76; N, 8.84. Found: C, 32.93; H, 3.00; N, 8.72.

[Rh(κ^3-Bu-bpa)(CO)]PF$_6$ ([5]PF$_6$). *From reaction of* [*I*]PF_6 *with CO*: 100 mg [**1**]PF_6 was dissolved in 10 mL of CH_3CN, and a stream of CO was bubbled through the solution for 10 min. [**2**]PF_6 was isolated in nearly quantitative yield by evaporation of the solvent.

From reaction of Bu-bpa with [{$(CO)_2Rh(\mu$-$Cl)\}_2$]: 110 mg (0.283 mmol) of [{$(CO)_2Rh(\mu$-Cl)}$_2$] and 140 mg (0.548 mmol) of Bu-bpa were dissolved in 20 mL of MeOH. The resulting orange solution was stirred for 1 h at rt and filtered. A solution of 350 mg of NH_4PF_6 in 5 mL of MeOH was added. Partial evaporation of the solvent caused the precipitation of [**3**]PF_6 as a yellow solid. Yield: 180 mg (0.339 mmol, 60.0%). ^{1}H NMR (400.14 MHz, CD_3CN): δ 8.33 (d, ^3J(H,H) = 6.7 Hz, 2H, Py-H6), 7.88−7.33 (m, 6H, Py-H3, Py-H4, Py-H5), 4.80 (d[AB], ^3J(H,H) = 16.0 Hz, N-CH_2-Py), 4.21 (d[AB], ^3J(H,H) = 16.0 Hz, N-CH_2-Py), 2.76 (m, 2H, N-CH_2-C_3H_7), 1.43 (m, 2H, N-CH_2-CH_2-C_2H_5), 1.14 (m, 2H, N-C_2H_4-CH_2-CH_3), 0.67 (t, ^3J(H,H) = 8.6 Hz, 3H, N-C_3H_6-CH_3). ^{13}C NMR (100.61 MHz, CD_3CN, 298 K): δ 190.0 (d, ^1J(Rh,C) = 79.1 Hz, CO), 164.2 (Py-C2), 154.6 (Py-C6), 140.2 (Py-C4), 126.0 (Py-C3), 124.1 (Py-C5), 66.5 (N-CH_2-Py), 62.1 (N-CH_2-C_3H_7), 26.7 (N-CH_2-CH_2-C_2H_5), 21.0 (N-C_2H_4-CH_2-CH_3), 14.0 (N-C_3H_6-CH_3). FT-IR (CH_3CN, cm^{-1}): $\nu_{(C\equiv O)}$ = 1994 cm^{-1}. FAB-MS: m/z 386 [M − PF_6]$^+$, 917 [2M − PF_6]$^+$. Anal. Calcd ($C_{17}H_{21}N_3RhOPF_6$): C, 38.44; H, 3.98; N, 7.91. Found: C, 38.54; H, 4.09; N, 7.89.

[Rh$_2$((μ-(bis-κ^3)tpen)(cod)$_2$](PF$_6$)$_2$ ([8](PF$_6$)$_2$). A 271 mg sample of [Rh(cod)(μ-Cl)]$_2$ (0.550 mmol) was suspended in 50 mL of MeOH, and 221 mg (0.520 mmol) of tpen was added. The solution was stirred for 1 h, after which the unreacted [Rh(cod)-(μ-Cl)]$_2$ was filtered off. Excess NH_4PF_6, dissolved in 8 mL of MeOH, was added. The yellow precipitate was filtered, washed with a small amount of methanol, and dried *in vacuo*. Yield: 504 mg (0.443 mmol, 85.2%). ^{1}H NMR (400.14 MHz, CD_3CN): δ 9.03 (d, ^3J(H,H) = 5.2 Hz, 4H, Py-H6), 7.70 (dt, 4H, ^3J(H,H) = 7.7 Hz, ^3J(H,H) = 1.3 Hz, Py-H4), 7.29 (t, ^3J(H,H) = 6.1 Hz, 4H, Py-H5), 7.25 (d, ^3J(H,H) = 7.4 Hz, 4H, Py-H3), 4.58 (d[AB], ^2J(H,H) = 16.3 Hz, 4H, N-CH_2-Py), 4.30 (d[AB], ^2J(H,H) = 16.3 Hz, 4H, N-CH_2-Py), 4.57 (s, 4H, N-CH_2-CH_2-N), 3.77 (s, 8H, CH=CH);

(35) Ahlrichs, R. *Turbomole Version 5*; Theoretical Chemistry Group, University of Karlsruhe, 2002.
(36) *PQS version 2.4*; Parallel Quantum Solutions: Fayetteville, AR, 2001. The Baker optimizer is available separately from PQS upon request: Baker, J. *J. Comput. Chem.* 1986, 7, 385−395.
(37) Sierka, M.; Hogekamp, A.; Ahlrichs, R. *J. Chem. Phys.* **2003**, *118*, 9136–9148.
(38) (a) Becke, A. D. *Phys. Rev. A* **1988**, *38*, 3098–3100. (b) Perdew, J. P. *Phys. Rev. B* **1986**, *33*, 8822–8824.
(39) Schaefer, A.; Horn, H.; Ahlrichs, R. *J. Chem. Phys.* **1992**, *97*, 2571–2577.

2.49 (m, 8H; CH_2), 1.80 (m, 8H; CH_2). ^{13}C NMR (100.61 MHz, CD_3CN, 298 K): δ 160.1 (Py-C2), 151.8 (Py-C6), 139.5 (Py-C4), 125.5 (Py-C3), 124.3 (Py-C5), 77.1 (d, ^1J(Rh,C) = 13.3 Hz; (CH=CH)), 63.7 (N-CH_2-Py), 58.9 (N-*CH_2-CH_2*-N), 31.7 (CH_2). Anal. Calcd ($C_{42}H_{52}N_6Rh_2P_2F_{12}$): C, 44.38; H, 4.61; N, 7.39. Found: C, 44.29; H, 4.65; N, 7.33.

[Rh_2((μ-(bis-κ^3)tppn)(cod)$_2$](PF_6)$_2$ ([9](PF_6)$_2$). A 147 mg amount of [Rh(cod)(μ-Cl)]$_2$ (0.298 mmol) was suspended in 50 mL of MeOH, and 119 mg (0.271 mmol) of tppn was added. The solution was stirred for 1 h, after which the unreacted [Rh(cod)(μ-Cl)]$_2$ was filtered off. Excess NH_4PF_6, dissolved in 4 mL of MeOH was added. The yellow precipitate was filtered, washed with a small amount of methanol, and dried *in vacuo*. Yield: 226 mg (0.196 mmol, 72.3%). ^{1}H NMR (400.14 MHz, CD_3CN): δ 9.08 (d, ^3J(H,H) = 5.0 Hz, 4H, Py-H6), 7.65 (dt, 4H, ^3J(H,H) = 7.2 Hz, ^3J(H,H) = 1.3 Hz, Py-H4), 7.23 (t, ^3J(H,H) = 7.6 Hz, 4H, Py-H5), 7.15 (d, ^3J(H,H) = 7.7 Hz, 4H, Py-H3), 4.51 (d[AB], ^2J(H,H) = 16.0 Hz, 4H, N-CH_2-Py), 4.16 (d[AB], ^2J(H,H) = 16.0 Hz, 4H, N-CH_2-Py), 4.15 (d, ^2J(H,H) = 16.0 Hz 4H, N-*CH_2*−), 3.79 (s, 8H, CH=CH); 2.65 (m, 8H; CH_2), 2.61 (m, 2H, N-CH_2-C*H_2*-CH_2-N2), 1.80 (m, 8H; CH_2). ^{13}C NMR (100.61 MHz, CD_3CN, 298 K): δ 160.1 (Py-C2), 152.0 (Py-C6), 139.3 (Py-C4), 125.2 (Py-C3), 124.1 (Py-C5), 76.7 (d, ^1J(Rh,C) = 13.5 Hz; (CH=CH)), 63.3 (N-CH_2-Py), 61.6 (N-*CH_2*-), 31.7 (CH_2), 21.1 (N-CH_2-*CH_2-CH_2*-N). FAB-MS: *m*/*z* 1005 [M − PF_6]$^+$, 1151 [M + H]$^+$, 1173 [M + Na]$^+$. Anal. Calcd ($C_{43}H_{54}N_6Rh_2P_2F_{12}\cdot H_2O$): C, 44.19; H, 4.83; N, 7.19. Found: C, 44.04; H, 4.62; N, 7.37.

[Rh_2((μ-(bis-κ^3)tpen)(CO)$_2$](PF_6)$_2$ ([11](PF_6)$_2$). A 121 mg amount of [Rh(CO)$_2$(μ-Cl)]$_2$ (0.313 mmol) was suspended in 50 mL of MeOH, 132 mg (0.311 mmol) of tpen was added, and the dark bordeaux-red solution was stirred for 1 h, after which the color changed to orange. Excess NH_4PF_6, dissolved in 5 mL of MeOH, was added. The red-brown precipitate was filtered, washed with a small amount of methanol, and dried *in vacuo*. The color of the solid turned to black upon drying and gave an orange solution upon dissolution in acetonitrile. Yield: 243 mg (0.250 mmol, 80.4%). ^{1}H NMR (400.14 MHz, CD_3CN): δ 8.24 (d, ^3J(H,H) = 5.5 Hz, 4H, Py-H6), 7.89 (t, 4H, ^3J(H,H) = 7.8 Hz, Py-H4), 7.33 (t, ^3J(H,H) = 6.5 Hz, 4H, Py-H5), 7.26 (d, ^3J(H,H) = 7.8 Hz, 4H, Py-H3), 4.79 (d[AB], ^2J(H,H) = 16.0 Hz, 4H, N-CH_2-Py), 4.11 (d[AB], ^2J(H,H) = 16.0 Hz, 4H, N-CH_2-Py), 3.13 (s, 4H, N-*CH_2*-). ^{13}C NMR (100.61 MHz, CD_3CN, 298 K): δ 190.0 (d, ^1J(Rh,C) = 67.5 Hz; (CO)), 163.0 (Py-C2), 154.9 (Py-C6), 140.4 (Py-C4), 126.4 (Py-C3), 124.4 (Py-C5), 66.8 (N-CH_2-Py), 59.2 (N-*CH_2*-). FT-IR (CH_3CN, cm^{-1}): $\nu_{(C\equiv O)}$ = 1999 cm^{-1}. Anal. Calcd ($C_{28}H_{28}N_6O_2Rh_2P_2F_{12}$): C, 35.45; H, 2.89; N, 8.61. Found: C, 35.17; H, 3.11; N, 8.87.

[Rh_2((μ-(bis-κ^3)tppn)(CO)$_2$](PF_6)$_2$ ([12](PF_6)$_2$). A 100 mg amount (0.257 mmol) of [{(CO)$_2$Rh(μ-Cl)}$_2$] and 110 mg (0.251 mmol) of tppn were dissolved in 20 mL of MeOH. The resulting orange solution was stirred for 1 h at rt and filtered. A solution of 350 mg of NH_4PF_6 in 5 mL of MeOH was added. Partial evaporation of the solvent caused the precipitation of [**4**](PF_6)$_2$ as a yellow solid. Yield: 183 mg (0.185 mmol, 74%). ^{1}H NMR (200.13 MHz, CD_3CN): δ 8.20 (d, ^3J(H,H) = 6.7 Hz, 4H, Py-H6), 7.99−7.33 (m, 12H, Py-H3, Py-H4, Py-H5), 4.80 (d[AB], ^3J(H,H)= 16.0 Hz, 4H, N-CH_2-Py), 4.18 (d[AB], ^3J(H,H) = 16.0 Hz, 4H, N-CH_2-Py), 2.80 (t, ^3J(H,H) = 6.6 Hz, 4H, N-*CH_2*-CH_2-), 1.90 (p, ^3J(H,H) = 6.6 Hz, 2H, N-CH_2-*CH_2*-). ^{13}C NMR (100.61 MHz, CD_3CN, 298 K): δ 190.0 (d, ^1J(Rh,C) = 79.0 Hz, CO), 163.9 (Py-C2), 154.7 (Py-C6), 140.3 (Py-C4), 126.2 (Py-C3), 121.7 (Py-C5), 66.8 (N-CH_2-Py), 60.5 (N-*CH_2*-CH_2-), 29.4 (N-CH_2-*CH_2*-). FT-IR (CH_3CN, cm^{-1}): $\nu_{(C\equiv O)}$ = 1994 cm^{-1}. FAB-MS: *m*/*z* 845 [M − PF_6]$^+$, 700 [M − 2PF_6]$^+$. Anal. Calcd ($C_{29}H_{30}N_6Rh_2O_2P_2F_{12}$): C, 35.17; H, 3.05; N, 8.49. Found: C, 34.90; H, 3.09; N, 8.39.

[Rh_2((μ-(bis-κ^3)tppn)]{(μ-CO)$_3$)$_2$}(PF_6)$_4$ ([13](PF_6)$_4$). A solution of 100 mg of [**4**](PF_6)$_2$ in 5 mL of CH_3CN was kept under 50 bar of CO for 4 days. Evaporation of the solvent yielded [**5**](PF_6)$_4$ as a yellow solid. ^{1}H NMR indicated the presence of only traces of [**4**](PF_6)$_2$ and almost quantitative yield of [**5**]-(PF_6)$_4$. ^{1}H NMR (300.13 MHz, CD_3CN): δ 8.69 (d, ^3J(H,H) = 5.2 Hz, 8H, Py-H6), 7.99−7.40 (m, 24H, Py-H3, Py-H4, Py-H5), 4.80 (d[AB], ^3J(H,H) = 16.0 Hz, 16H, N-CH_2-Py), 4.18 (d[AB], ^3J(H,H) = 16.0 Hz, 16H, N-CH_2-Py), 2.80 (t, ^3J(H,H) = 7.9 Hz, 8H, N-*CH_2*-CH_2-), 1.90 (p, ^3J(H,H) = 7.9 Hz, 4H, N-CH_2-*CH_2*-). ^{13}C NMR (75.47 MHz, CD_3CN, 298 K): δ 214.9 (t, ^1J(C,Rh) = 29.1 Hz, μ_2-CO), 213.1 (t, ^1J(C,Rh) = 29.1 Hz, μ_2-CO), 160.1 (Py-C2), 150.1 (Py-C6), 141.4 (Py-C4), 126.3 (Py-C3), 125.0 (Py-C5), 65.4 (N-CH_2-Py), 63.5 (N-*CH_2*-CH_2-), 17.7 (N-CH_2-*CH_2*-). IR (CsI): $\nu_{(C\equiv O)}$ = 1838 (s), 1825 (sh) cm^{-1}. IR (CH_3CN): $\nu_{(C\equiv O)}$ = 1838 (s), 1828 (sh) cm^{-1}. FAB-MS: *m*/*z* 1891 [M − PF_6]$^+$, 1835 [M − CO − PF_6]$^+$. Calcd for [[**5**](PF_6)$_3$]$^+$ ($C_{60}H_{60}N_{12}Rh_4O_6P_3F_{18}$) *m*/*z* 1890.990439; found *m*/*z* 1891.004300 (Δ = −7.3).

[Rh(κ^3-tpa)(CO)]PF_6 ([14]PF_6). A 197 mg amount of [Rh(μ-Cl)(coe)$_2$]$_2$ (0.275 mmol) was suspended in 10 mL of MeOH, and 167 mg of tpa (0.575 mmol) was added. CO was bubbled until all the solid dissolved and the solution turned yellow-brown. The solution was stirred for additional 20 min under CO atmosphere, after which 143 mg of KPF_6 (0.781 mmol) was added, causing precipitation of a yellow solid, which was filtered off and washed twice with 2 mL of MeOH. Yield: 213 mg (0.376 mmol). Compound was recrystallized from 10 mL of hot MeOH to yield 140 mg (0.247 mmol, 45.0%) of analytically pure product.

After dissolution of $\mathbf{14}^+$ in acetone, compound $\mathbf{14}^+$ exists in equilibrium with $\mathbf{15}^{2+}$. Signals of $\mathbf{15}^{2+}$ were omitted for clarity. Py^C = coordinated picolyl moiety, Py^D = dangling picolyl moiety. ^{1}H NMR (500 MHz, acetone-d_6, −5 °C): δ 8.44 (d, ^3J(H,H) = 5.0 Hz, 2H; Py^C-H6); 8.35 (d, ^3J(H,H) = 3.5 Hz, 1H; Py^D-H6); 8.02 (t, ^3J(H,H) = 7.5 Hz, 2H; Py^C-H4); 7.98 (d, ^3J(H,H) = 7.5 Hz, 1H; Py^D-H3); 7.65 (t, ^3J(H,H) = 7.5 Hz, 1H; Py^D-H4); 7.61 (d, ^3J(H,H) = 8.0 Hz, 2H; Py^C-H3); 7.40 (t, ^3J(H,H) = 7.0 Hz, 2H; Py^C-H5); 7.14 (t, ^3J(H,H) = 6.0 Hz, 1H; Py^D-H5); 5.23 (d[AB], ^2J(H,H) = 15.5 Hz, 2H; N−CH_2-Py^C); 4.84 (d[AB], ^2J(H,H) = 15.5 Hz, 2H; N-CH_2-Py^C); 4.38 (s, 2H; N-CH_2-Py^D). ^{13}C NMR (125 MHz, acetone, −27 °C): δ 190.8 (d, ^1J(Rh,C) = 79.5 Hz; (CO)); 165.1 (Py^C); 155.3 (Py^C); 155.2 (Py^D); 154.2 (Py); 151.1 (Py^D); 150.9 (Py^D); 140.7 (Py^C); 138.0 (Py^D), 129.5 (Py); 129.3 (py); 66.4 (N-CH_2-Py); 65.9 (N-CH_2-Py). IR (MeCN): $\nu_{(C\equiv O)}$ = 1991 cm^{-1}. Anal. Calcd ($C_{19}H_{18}F_6N_4OPRh$): C, 40.30; H, 3.20; N, 9.89. Found: C, 40.63; H, 3.57; N, 9.83

[Rh(κ^3-tpa)(CO)]B(*m*-xylyl)$_4$ ([14] B(*m*-xylyl)$_4$). Complex $\mathbf{14}^+$ with B(*m*-xylyl)$_4^-$ and B(*m*-tolyl)$_4^-$ counterions could also be obtained by reaction of corresponding ethene complexes[40] with CO in the solid state. ^{1}H NMR (CD_2Cl_2, 200 MHz, v br): δ 8.14 (s, 2H); 7.65 (m, 2H); 7.42 (s, 2H); 7.16 (s, 8H); 6.97 (d, 6H); 6.54 (s, 4H); 3.61 (s, 2H); 3.12 (d, 4H); 2.09 (s, 24H). IR (KBr): $\nu_{(C\equiv O)}$ = 1990 cm^{-1}. Calcd mass for $\mathbf{14}^+$ ($C_{19}H_{18}N_4ORh$) 421.05357; accurate mass 421.05274 (Δ = 1.90).

[Rh(κ^4-tpa)(CO)]$_2$(PF_6)$_2$ ([15](PF_6)$_2$). After dissolution of $\mathbf{14}^+$ in acetone, compound $\mathbf{15}^{2+}$ exists in equilibrium with $\mathbf{14}^+$. Signals of $\mathbf{14}^+$ were omitted for clarity. ^{1}H (500 MHz, acetone-d_6, −5 °C): δ 8.52 (d, ^3J(H,H) = 5.0 Hz, 3H; Py-H6); 7.82 (d, ^3J(H,H) = 7.5 Hz ^4J(H,H) = 1.0 Hz, 3H; Py-H4); 7.46 (d, ^3J(H,H) = 7.5 Hz, 3H; Py-H3); 7.25 (t, ^3J(H,H) = 6.5 Hz, 3H; Py-H5); 5.08 (s, 6H; N-CH_2-Py). ^{13}C (125 MHz, acetone, −60 °C, all peaks broad): δ 208.3 (t, ^1J(Rh,C) = 19.6 Hz; (CO)); 162.5 (Py); 153.2 (Py); 140.4 (Py); 140.1 (Py); 126.4 (Py); 126.1 (Py); 125.2 (Py); 65.7 (N-CH_2-Py). IR (MeCN): $\nu_{(C\equiv O)}$ = 1749 cm^{-1}.

[Rh(κ^4-tpa)(CO_3)]B(*m*-xylyl)$_4$ ([16] B(*m*-xylyl)$_4$). Rh(tpa)-(CO)B(*m*-xylyl)$_4$ (50 mg) was put in an atmosphere 50/50 O_2/N_2 for 2 days. The product was obtained as an off-white solid. Yield: >95%. Crystals suitable for X-ray diffraction were obtained by diffusion of hexane into a solution of dichloromethane. ^{1}H NMR (CD_2Cl_2, 400 MHz): δ 8.82

(40) [Rh(tpa)(ethene)]B(*m*-xylyl)$_4$ and [Rh(tpa)(ethene)]B(*p*-tolyl)$_4$ were prepared using a method described for [Rh(tpa)(ethene)]BPh_4: de Bruin, B.; Boerakker, M. J.; Verhagen, J. A. W.; de Gelder, R.; Smits, J. M. M.; Gal, A. W. *Chem.−Eur. J.* **2000**, *6*, 298–312.

(dd, ^3J(H,H) = 5.7 Hz, ^4J(H,H) = 0.7 Hz, 1H; Py^A-H6), 8.50 (d, J = 5.6 Hz, 2H Py^B-H6), 7.87 (dt, J = 7.8 Hz, J = 1.6 Hz, 2H), 7.63 (dt, J = 7.8 Hz, J = 1.5 Hz, 1H), 7.41 (dd, J = 8.1 Hz, J = 6.5 Hz, 3H), 7.34(dd, J = 7.8 Hz, J = 5.8 Hz, 3H), 7.25 (d, J = 7.9 Hz, 2H), 7.13 (s, 8H), 6.80 (d, J = 7.7 Hz; 1H), 6.52 (s, 4H), 4.51 (d[AB], J = 16.0 Hz, 2H), 3.93 (d[AB], J = 15.9 Hz, 2H), 3.85 (s, 2H), 2.09 (s, 24H). ^{13}C NMR (CD_2Cl_2, 400 MHz): δ 166.2 (M-CO_3), 164.4 (q, ^1J(B,C) = 49 Hz, BAr-C1), 161.4 (Py^B-C2), 159.7 (Py^A-C2), 150.1 (Py^B-C6), 149.4 (Py^B-C6), 140.7 (Py^B-C4), 140.1 (Py^A-C4), 134.2 (BAr-C2/3), 126.5 (Py^B-C3/5), 126.1 (Py^A-C3/5), 123.9 (Py^B-C3/5), 123.8 (Py^A-C3/5), 122.0 (BAr-C4), 69.6 (N-CH_2-Py^B), 67.9 (N-CH_2-Py^A), 22.0 (BAr-Me). IR (KBr) (cm^{-1}): $\nu_{C=O}$ = 1690, 1661, 1631; ν_{C-O} = 1205 (C−O) (the observation of multiple C=O bands is probably caused by different H-bonding moieties with water). MS (ESI/acetone): 453 [M − B(m-xylyl)$_4$]$^+$. Calcd mass ($C_{19}H_{18}N_4O_3Rh$) 453.04339; accurate mass 453.04119 (Δ = 4.79).

Acknowledgment. We thank The Netherlands Organization for Scientific Research−Chemical Sciences (NWO-CW VIDI project 700.55.426), the European Research Counsel (Grant Agreement 202886), the Radboud University of Nijmegen, and the University of Amsterdam (UvA) for financial support. We thank Jan Meine Ernsting for his assistance with the low-temperature NMR experiments. Ferry van Nisselroij and Caroline Schouten are acknowledged for the synthesis of some of the described compounds.

Supporting Information Available: Crystallographic information (cif file) containing data for complexes **2**, **8**, **15**, and **16**. The crystal structures were also deposited with the CCDC (deposition numbers CCDC767613-767616). DFT-optimized geometries of compounds **9** and **13**. VT-NMR spectrum of species **14**$^+$ in dichloromethane. This material is available free of charge via the Internet at http://pubs.acs.org.